Processing of harmonic type DP microstructures in the given steel and investigating deformation behavior through tensile testing and also by modelling-simulation.

A Dissertation submitted

in fulfillment of the requirements

for the Degree of

Master of Engineering

in

Production Engineering

By

HARMANPREET SINGH

Regd. No. 801685007

Under Supervision of:

Dr. Tarun Nanda
Associate Professor, MED
TIET, Patiala

Dr. B. Ravi Kumar
Sr. Principal Scientist, MTE
CSIR-NML, Jamshedpur

MECHANICAL ENGINEERING DEPARTMENT
THAPAR INSTITUTE OF ENGINEERING AND TECHNOLOGY
(A DEEMED TO BE UNIVERSITY), PATIALA-147004, PUNJAB, INDIA
JULY, 2018

CERTIFICATE

I, Harmanpreet Singh, hereby declare that the work presented in this thesis entitled **"Processing of harmonic type DP microstructures in the given steel and investigating deformation behavior through tensile testing and also by modelling-simulation"** in fulfillment of the requirements for the award of degree of Master of Engineering (Production Engineering) submitted to Department of Mechanical Engineering, **Thapar Institute of Engineering and Technology, Patiala** is an authentic record of work carried out under the supervision of **Dr. Tarun Nanda**, Associate Professor, TIET, Patiala and **Dr. B. Ravi Kumar**, Senior Principal Scientist, CSIR-NML, Jamshedpur from July 2016 to 2018. The matter presented in this report has not been submitted either in part or full to any other university or institute for the award of any degree.

Harmanpreet Singh

(Harmanpreet Singh)

Date: 10.08.2018

Tarun Nanda

Dr. Tarun Nanda
Associate Professor
Department of Mechanical engineering
TIET, Patiala

Ravikumar

Dr. B. Ravi Kumar
Senior Principal Scientist
MTE Division
CSIR-NML, Jamshedpur

ACKNOWLEDGEMENT

I would like to express my deepest sense of gratitude and a very sincere thanks to my guide Dr. Tarun Nanda, Associate Professor, Mechanical Engineering Department, Thapar Institute of Engineering and Technology, Patiala and Dr. B. Ravi Kumar**,** Senior Principal Scientist, CSIR-NML, Jamshedpur for their sincere and invaluable guidance and full support which helped me in the accomplishment of this thesis report in the present form. Their dynamic and diligent enthusiasm has been highly instrumental in keeping my spirits high. Their flawless and forthright suggestions blended with an innate intelligent application have crowned my task with success.

I also acknowledge the opportunity given to me for training in *National Metallurgical Laboratory*. My special thanks to all the technical staff of CSIR-NML, Jamshedpur for their ready assistance during my experimentation phase.

I am also thankful to Dr. T.P Singh, Head of Department, Mechanical Engineering, for providing us with the adequate infrastructure in carrying out the work. I would like to thank the entire faculty and staff of Mechanical Engineering Department and my friends who devoted their valuable time and help me in all possible ways towards successful completion of this work.

Lastly, I would like to thank my family for their years of guidance, support, and encouragement. It would not have been possible without them to reach up to this point. They have always wanted the best for me and I admire their determination and sacrifices.

HARMANPREET SINGH

ABSTRACT

Dual phase steels (DP steels) consist of martensite phase (hard phase to impart high strength) and ferrite phase (soft phase to provide elongation). These steels have been widely used in automobile units because of their good mechanical properties providing good strength-ductility combination. Now-a-days, research has focused on development of DP steels with lean composition. Parallel to this, new processing techniques have also been developed to control the microstructure evolution which further improves the strength-ductility combination. Controlled annealing is one of the techniques used to alter the ferrite-martensite morphology of DP steels with lean composition. The present dissertation work was an attempt to extend the concept of harmonic structure design on the microstructure of DP steels and to investigate its effect on the strength-ductility combination of the steels. In the present work, harmonic structures were developed in DP steels having soft-shell of ferrite phase (three-dimensional network structure) surrounding the hard-core martensite phase. Five different annealing cycles were used to get distinct DP microstructures having different martensite distribution and volume fraction. These five different cycles belonged to two broad annealing categories (i) Continuous Annealing Line (CAL process) and (ii) Core and Shell (CAS process). The tensile properties of steels with these different DP microstructures were evaluated using tensile testing. Experimental results showed that strength of steels increased with increase in martensite volume fraction in the DP microstructure. Also, for the dual phase steels with harmonic structure, steels containing higher martensite fraction and typical core and shell type microstructure showed very limited micro-cracking of martensite in the tensile necking zone. Further, ferrite-martensite interface and martensite inter-lath damage activity was restricted and both ferrite and martensite revealed plastic strain compatibility. In the second major part of this dissertation work, microstructures obtained by CAL and CAS (only one out of the four microstructures processed by CAS) routes were successfully modelled using Dream.3D software. Further, simulation results using Abaqus software were able to appropriately predict the deformation behavior of DP steels. Good agreement between predicted simulation results and experimental results was observed with regards to deformation behavior shown by different DP steels.

Keywords: Dual phase steels, Harmonic structure, Simulation, Modelling, Tensile properties.

Table of Contents

LIST OF FIGURES

LIST OF TABLES

NOMENCLATURE

Acronym	Full Form
AHSS	Advance High Strength Steel
DP	Dual Phase
LDP	Laminated Dual Phase
YS	Yield Strength
UTS	Universal Tensile Strength
TRIP	Transformation Induced Plasticity
SIP	Shear induced plasticity
TWIP	Twin Induced Plasticity
CP	Complex Phase
L-IP	Light weight induced plasticity
HSLA	High strength low alloyed
MVF	Martensite Volume Fraction
IHT	Inter-critical Holding Temperature
CAS	Core and Shell
SEM	Scanning Electron Microscopy
TEM	Transmission Electron Microscopy
EBSD	Electron Back Scatter Diffraction
FEA	Finite element analysis
HM	Harmonic
CAL	Continuous Annealing Line
CHCL	Continuous Heating and Cooling Line
DP-C	DP steel processed through CAL route

CHAPTER 1

INTRODUCTION

1.1 General

A newly developed category in steels is the Advanced High Strength Steels (AHSS). These steels have extensive applications in automobile industry. The proposed work is an attempt to investigate the influence on outcome (in terms of strength and ductility) in ferrite-martensite based dual phase steels (DP steels) by varying the distribution and volume fraction of martensite.

1.2 Dual Phase Steels

Dual phase steels (DP steels) are a category under AHSS. AHSSs provide superior ability to form along with good strength as compared to the high strength steels made through conventional methods. AHSS are steels possessing yield strength (YS) greater than 300 MPa and ultimate tensile strength (UTS) greater than 550 MPa. For tensile strengths greater than 780 MPa, AHSS are also called ultra-high strength steels [1–5]. The presence of multi-phase microstructures including ferrite-martensite, ferrite-bainite and/or retained austenite makes the AHSS family good in strength-formability combination [6–10].

The classification of AHSS is done in three generations. The first generation contains ferrite as the main phase and includes dual-phase (DP), complex-phase (CP), and transformation-induced-plasticity (TRIP) steels. AHSS steels are better than the conventionally used high strength low alloy (HSLA) steels in strength levels but formability of AHSS is inferior as compared to HSLA steels [7–11]. To overcome this problem of first generation, the second generation of AHSS was developed for superior strength-formability combination. The second generation includes light-weight-induced plasticity (L-IP), twinning-induced plasticity (TWIP), and shear-induced plasticity (SIP) steels. The second generation provides outstanding strength-formability but this comes at the high cost of alloying. Due to this, this generation is less preferred [10–15]. To obtain excellent strength and easily formable steel at low costs, the third generation was developed, wherein novel processing routes improved the mechanical properties. The superior strength-formability combination offered by third generation AHSS is a result of carefully selected chemical composition and specific microstructural morphologies obtained from controlled heating and cooling processes. DP, TRIP, and CP steels are modified to obtain newly developed third generation of advanced high strength steels [10, 12, 13, 16].

DP steels consist of widely spread martensite phase in a matrix of ferrite phase. These steels have excellent properties including superior strength-ductility and better formability as compared to conventionally used steel of same composition [17]. These developed steels come under the strength range of about 400–1000 MPa [7,17, 10]. In DP steels, ferrite forms the ductile and deformable constituent and the second phase bainite/martensite strengthens the steel [18,19].

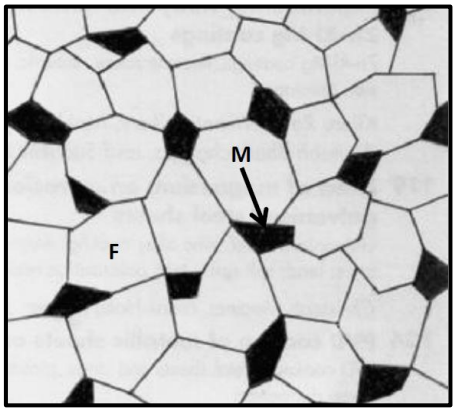

Figure 1.1 Island of martensite in a matrix of ferrite in DP steels. F=ferrite and M=martensite [19].

The composition of DP steels mainly consists of elements including C (0.05–0.2%), Mn (1.2–1.6%), Si (0.03–0.6). Micro-additions of V, Nb, Ti are done with concentration of about 0.1%. Martensite phase plays an important role in DP steels, where strength is dependent on volume fraction and ductile nature on morphology and proportion of martensite. The main advantage of this steel is that there is no elongation at yield point and it displays lower yield strength to ultimate tensile strength fraction (near to 0.5) [7]. Figure 2 presents the typical routes followed for processing DP steels.

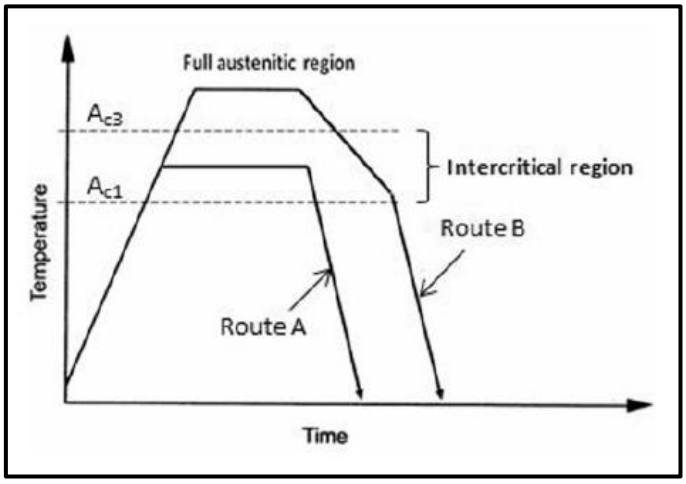

Figure 1.2 Processing routes of DP steels [7].

1.3 Modelling and Simulation

Modelling and simulation is the virtual experimentation done on computers similar to the physical experimentation. Here, the values of physical conditions of experimentation are same but are done on computers, so that we can visualize the results which depict the particular result with the color combinations, pre-defined in color scale in that particular simulation. Mostly the modelling is done through mathematical models which define all the physical parameters. The results obtained through computer in the form of simulations are approximate results which are similar to the physical experimental results. Nearly accurate results can be obtained through modelling and simulations if the meshing is very fine. However, fine meshing requires additional time and superior computer hardware like workstations etc.

1.4 Origin of the proposed work

Despite the several advantages offered by DP steels, there is scope for improvement in ductility. To obtain good strength-ductility combination in this AHSS category, the present work proposes to investigate the effect of change in second phase (martensite) fraction and distribution on the tensile properties of DP steels. In the present dissertation work, as-received low carbon cold-rolled steel was subjected to various annealing routes to obtain different DP microstructures in the steel. The objective was to investigate the influence of change in martensite fraction and distribution on strength and ductile nature of DP steels. The results have been initially obtained experimentally through tensile testing of steel of different microstructures. The work has been expanded further to analyze the difference in tensile deformation behavior and damage mechanisms in two different DP microstructures through modelling and simulation.

CHAPTER 2
LITERATURE REVIEW

2.1 International and national status

Adamczyk and Grajcar [20] investigated the effect of thermo-mechanical processing on microstructure/mechanical properties of dual phase steel. Steel of composition (0.09 C, 1.5 Mn, 0.26 Si, 0.07 Ni, 0.014 P, 0.009 S, 0.003 B, 0.029 Al, 0.012 N; all in wt. %) was melted and casted in 100×100 mm slabs. These slabs were hot rolled and forged into rods of section 24×24 mm. Three routes were followed for giving heat treatment to specimens, the steel was heated to 910 ℃ for 30 min in all the three routes. In route I, the specimen was air cooled to room temperature, then again heated to 750 ℃ and finally was water quenched. This led to formation of ferrite structure with an irregular envelope of martensite on grain boundaries. In route II, specimen was water quenched for both the temperatures (i.e. 910 ℃ and 750 ℃). After primary quenching when the steel was heated, nucleation of austenite mainly occurred on the boundaries of martensite laths. The predominated martensite fraction occurred mainly as thin fibers. Small grains of recrystallized ferrite could be identified in the surroundings of martensite. In route III, steel was austenized at 910 ℃ and then was air cooled for 45 s to a temperature of 750 ℃, followed by water quenching. Due to this processing, martensite was located on grain boundaries of the ferrite phase.

These conditions helped in obtaining DP steels of comparable fraction of ferrite (ferrite grain size: 7–10 μm) and martensite (MVF=21–24 %), but with varied martensite distribution and morphologies. These various morphologies of martensite affected the tensile deformation characteristics. The optimum strength-ductility combination was achieved by route II.

Calcagnotto *et al.* [21] studied the influence of grain size on properties of DP steels subjected to inter-critical annealing process (730 ℃, 3 min, quenching). Fine grained/ultra-fine grained (2.4 μm and 1.2 μm) steels were obtained with ferrite and martensite as the two phases (reference sample was coarse grained steel, 12.4 μm). MVF in coarse, fine, ultra-fine, and coarse-grained steels was 31.3%, 30.1%, and 29.8% respectively. Results showed that UTS and YS increase and ductility is affected marginally with decrease in grain size. It was concluded that grain refinement affects properties of dual phase steels and ultra-fine-grained DP steels provide better properties as compared to fine grained and coarse-grained DP steels.

Zuo *et al.* [22] studied the microstructure/properties of DP steel containing large MVF. Steel (0.37 C, 0.48 Si, 0.86 Mn, 1.67 Cr, 0.36 Mo, 0.015 P, 0.003 S; all in wt. %) was subjected to inter-critical annealing in the range 785–830 ℃.

DP microstructure was obtained from two different types of starting microstructures. The first was a "ferrite and pearlite" microstructure and DP steels processed from this starting microstructure were designated as series 'A' DP steels. The second type of DP microstructures were obtained from the initial "martensite" microstructure and were designated as series 'B' DP steels. For converting the starting microstructures into DP microstructures, the following process parameters were used: inter-critical temperatures selected were 785 ℃, 800 ℃, 815 ℃, 830 ℃ for 30 minutes and subsequent three different types of holding times (10, 30, 50 min) at 785 ℃.

With increase in heat treatment temperature and holding period, elongation decreased for both types of steels. B series steel showed higher strength/percent elongation when annealed under the following conditions: 785 ℃, 30 min and 800 ℃, 30 min.

Holloman equation ($\sigma_t = k\varepsilon_t^n$; σ_t: true stress, ε_t: true strain, k: strength coefficient, n: work hardening exponent) was used to describe the stress-strain behavior. With increase in heat treatment temperature and also soaking period, n and k increased. For initial strain levels (less than 0.5% strain), work hardening rate ($d\sigma_t/d\varepsilon_t$) was high which reduced at higher strains. Also, for low strains till 3%, B series showed greater work hardening rate than A type.

Ciuca *et al.* [23] studied the mechanical properties of SUS 329J1 by creating a harmonic structure (a typical DP microstructure) in a steel of composition, 29.8 Cr, 4.17 Ni, 1.76 Mo, 0.9 Mn, 0.27 C, 0.23 Si, 0.03 P, 0.02 N, 0.01 Cu (all in mass %). The particle size of powder was 135 μm. Properties of sintered powder were compared with bulk material.

Initially, the powder structure was milled in a planetary ball mill for 90 s at 200 rpm. It was then consolidated by spark-plasma sintering (50 MPa, 1123 K) to obtain sintered discs (diameter: 15 mm; thickness: ~ 4 mm).

Vickers hardness of initial powder, milled powder (center region), milled powder (surface region) was 332 VPN, 410 VPN, and 427 VPN respectively.

Figure 2.1 (EBSD analysis), showed a narrow micro-duplex structure (mild shell) and neighboring micro-duplex structure (outer shell) with grain size of 570 nm and 1.26 μm respectively. The reason of formation of two shells was precipitation behavior of the second phase, recovery, and recrystallization of the matrix phase.

YS and UTS of harmonic structure compact was significantly higher than the bulk material (40% and 25% more). Harmonic structure compact exhibited remarkable uniform elongation of ~17% along with higher strength levels.

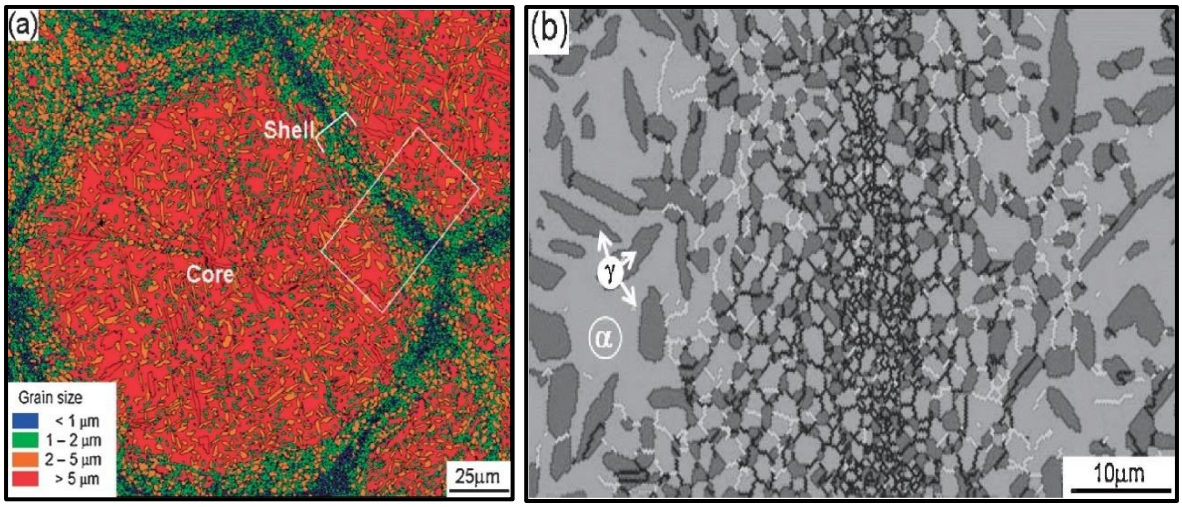

Figure 2.1 (a) Grain size map, and (b) phase map, showing harmonic structure [23].

Meng *et al.* [24] explored the possibility of fast-heating routine (FA) of cold rolled sheets (Fe –0.07C, –1.7Mn, –0.429Si; 70 % cold reduction) for large scale production. For comparison, DP steel processed by CAL route was also taken. From the dilatometer study, the lower and upper critical temperatures were found out to be 1023 K and 1193 K respectively (for 500 K/s as heating rate). Specimen was heated to 1123 K, soaked for 2 s, cooled to 323 K. Microstructure evaluation and tensile testing was done for both the steels i.e. fast heated (FH) and continuous annealed (CAL). Tensile tests showed that YS (227 MPa to 372 MPa), UTS (625 MPa to 666 MPa), and even percentage elongation (23.3% to 26.6%) increased for the FA route. Compared to the continuous annealed sample, the ferrite grains were observed to be refined strikingly in the fast-heated sample. The fine and fibrous morphology of the martensite in the FH sample resulted in improvement of strength. Hence, it was concluded that the simplified fast heating process can be an alternative route for the production of dual phase steels.

Saeidi *et al.* [25] developed a novel category of DP steel (laminated dual phase, LDP steel). In this study, production method of LDP and its comparison with DP600 was discussed.

Two types of steels St37 and IF steels were used here to produce LDP steel. St37 contained high carbon content (0.13% C) and was used as middle layer (ML) placed between 2 IF steel sheets. So, IF sheets (0.002% C) formed the outer layer (OL). Figure 2.2 shows the schematic of new processing method of LDP.

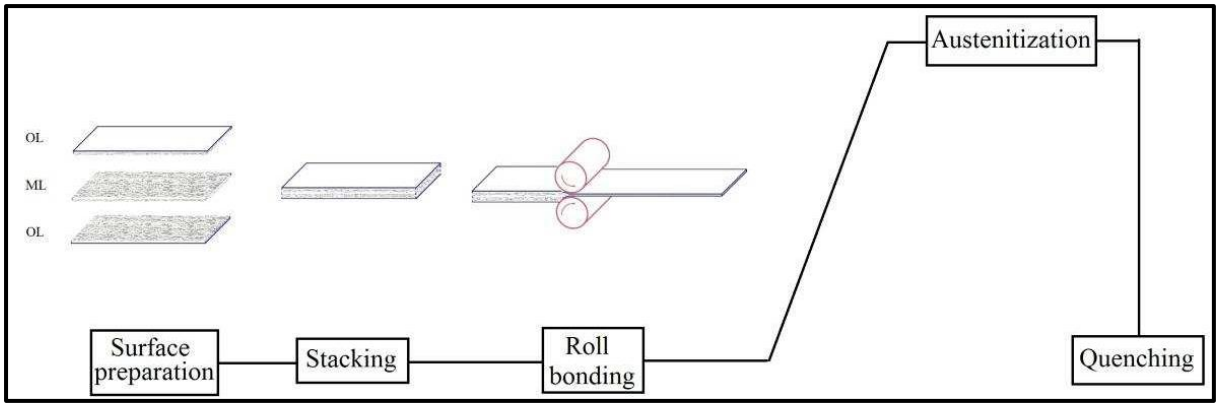

Figure 2.2 Processing for laminated DP steel [25].

Table 2.1 presents the properties of the steels respectively. The austenization temperature was 850 $°C$ with 7 min of holding, followed by quenching in water.

Table 2.1 Properties of layers [25].

Layer	YS (MPa)	TS (MPa)	TE (%)
ML Steel	235±10	360±8	16±1
OL Steel	83±5	220±10	51±1

The middle layer (ML) was converted to dual phase microstructure comprising of martensite-ferrite phases (mainly martensite with few grains of ferrite). On the contrary, OL layers, which contained very less carbon, obtained a fully ferritic microstructure.

SEM images depicted that in ML/OL interface, there was resistance against void initiation and growth, and therefore they remained unchanged. For the region adjoining fractured surface, it was observed that fracture got initiated from ML/OL interface under conditions of high strain (0.86). At interfaces of ML/OL, large re-crystallized ferrite grains were noticed.

YS of LDP steel was comparable to that of DP600, UTS was low, but elongation was identical (see Table 2.2).

Table 2.2 Properties of various steels [25].

Specimen	Tensile Strength (MPa)	Total Elongation (%)	Uniform Elongation (%)
LDP	540±7	20±1.5	16±0.2
DP600	633	24	16

Thus, it was concluded that the new LDP method could be used in place of thermo-mechanical route.

Ota *et al.* [26] investigated the properties of steel by preparing harmonic structured steel. Steel chemistry included 25 Cr, 4.5 Ni, 2 Mo, balance Fe, all in wt. %. The powder was initially in fully ferritic state with particle size of 280 µm which was mechanically milled at 200 rpm for 90 ks under Ar atmosphere. The powder was subjected to sintering (1123 K, 1.8 ks, 50 MPa). Figure 2.3 shows the tensile test results of the three types of specimens (a) conventional bulk duplex steel, (b) compacts of as-received powders, (c) and compacts with harmonic structure. Compacts prepared from powder showed similar YS and UTS but low percent elongation as compared to duplex steel. Harmonic structured compacts showed significantly increased YS and UTS compared to the other steels. Percentage elongation of harmonic structured compacts was also comparable to conventional material. Harmonic structured duplex steel compacts exhibited uniform elongation along with strengthening.

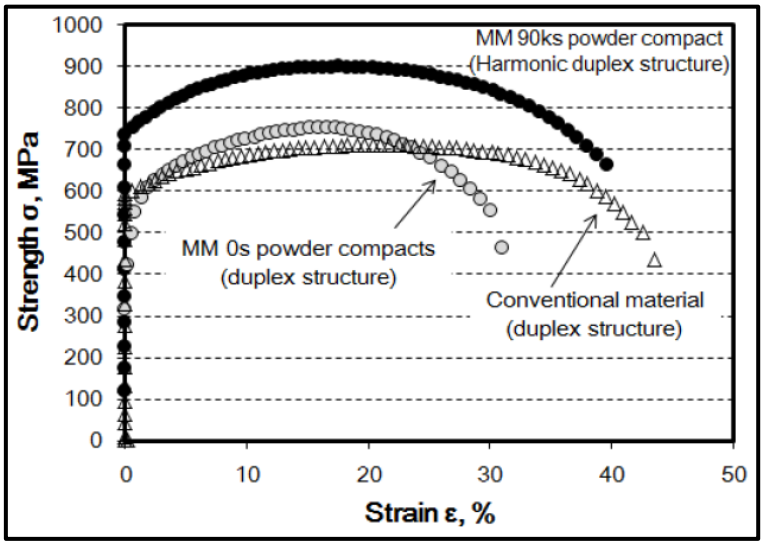

Figure 2.3 Tensile test results for the three materials [26].

Thus, harmonic structured design showed high strength and good ductility combination.

Wang *et al.* [27] prepared ultra-fine grained (UFG) microstructure by annealing a low carbon steel of composition (C 0.12, Si 0.24, Mn 1.42, P 0.012, S 0.004, Nb 0.014, all in wt. %). Starting material was austenized (1000 ℃, 30 min), cooled (760 ℃, 30 min), and rapidly quenched. DP microstructure with martensite (MVF = 60%) and ferrite was obtained. Further, the sample was cold rolled (64% reduction) in six passes. It was then annealed (560 ℃, different times). The resulting structure contained recrystallized ferrite with bimodal grain size distribution and carbides of size 60 nm. YS, UTS, UE, and TE values were 663 MPa, 788 MPa, 17.8%, and 21.6% respectively. Larger grains help in movement and accumulation of dislocations and enhance percentage elongation. Ultra-fine grains promote strength. The

carbides increased strength as well as percent elongation by increasing dislocation density and work hardening rate.

Apart from the above reviews, some other authors like Ueinishi *et al.* [5], Matlock *et al.* [12], Maggi *et al.* [14] have also worked to study the effect of martensite morphology on mechanical properties of DP steels.

Sudersanan *et al.* [28] studied the variations in properties of DP steels with variation of carbon content in second phase martensite present in DP microstructure. Chemical composition (0.13 C, 1.18 Mn, 0.01 S, 0.001 P, 0.3 Si, 0.047 Cr, 0.057 Mo, 0.001 B, 0.048 Ni all in wt. %) was used. The specimens were heat treated in the temperature range of 730 ℃ to 810 ℃, to obtain different volume fractions of martensite in DP structure. MVF was higher at higher annealing temperatures. The carbon content in the martensite decreased at higher martensite fractions. Yield strength and ultimate tensile strength increased with increase in carbon content in martensite to a certain limit. YS and UTS increased initially with carbon content till 0.195% and then decreased with increase in carbon content in the martensite phase.

Han *et al.* [29] examined strain partitioning of ferrite and martensite phases of DP steels, both experimentally as well as numerically through FE modelling. As received material (0.104 C, 0.92 Si, 2.01 Mn, 0.03 Cr, 0.03 Al, 0.019 Al; all in wt. %) was solution treated (920 ℃, 8 min) followed by annealing (730 ℃, 5 min) and then water quenching. This was followed by tempering (280 ℃, 450 ℃, 500 ℃ and 550 ℃, 10 min). MVF was 54%.

Nano hardness with 14*14 arrays (distance of 50 μm) was taken. Hardness was measured for each phase for tempered samples and also for pre-strained samples (2% and 5%). The equation, $\sigma = K\varepsilon^n$ was fitted to nanohardness data. Higher temperature used for tempering decreased strength but improved ductility. Ferrite showed slight softening and martensite showed large decrease in hardness due to tempering. Results showed that for DP microstructure, strain experienced by softer phase is significantly higher than macroscopic strain. SEM micrographs showed void formation, nucleation, and growth at ferrite-martensite interface and fracture of martensite as the main damage mechanisms. FE simulations showed (a) stress-strain response of the simulated volume for imposed deformation (Figure 2.4) and (b) strain distribution in simulated microstructure.

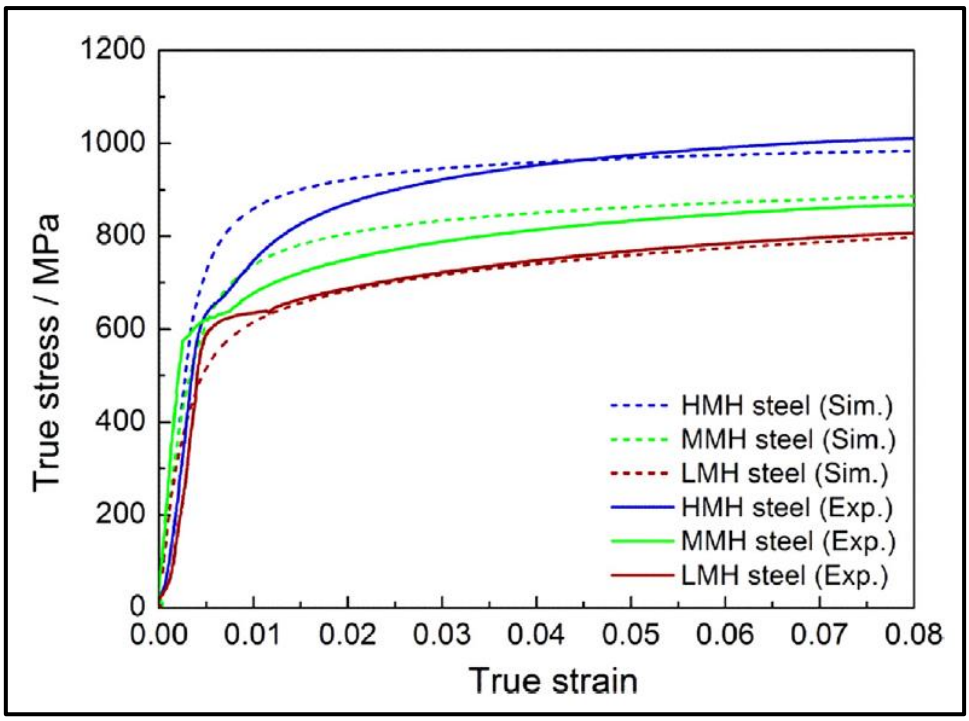

Figure 2.4 Simulation and experimental results [29].

Modelling results showed that deformation produced localised regions of extremely high strain within ferrite and also those of minimal strain. So if constituent phases have differences in strength, such diverse strain regions are observed. If constituent phases have similar properties, strain will still partition, more strongly to the softer phase.

Kumar *et al.* [30] proposed a new approach for studying the deformation behaviour/failure criteria of Al-SiC composite by developing a two-dimensional model.

The microstructure image was in the raster form (Figure 2.5). It was converted into vector format (Figure 2.6) by Win Topo software. It is an image processing technique in which edge detection method for detecting edges of SiC particles was utilized.

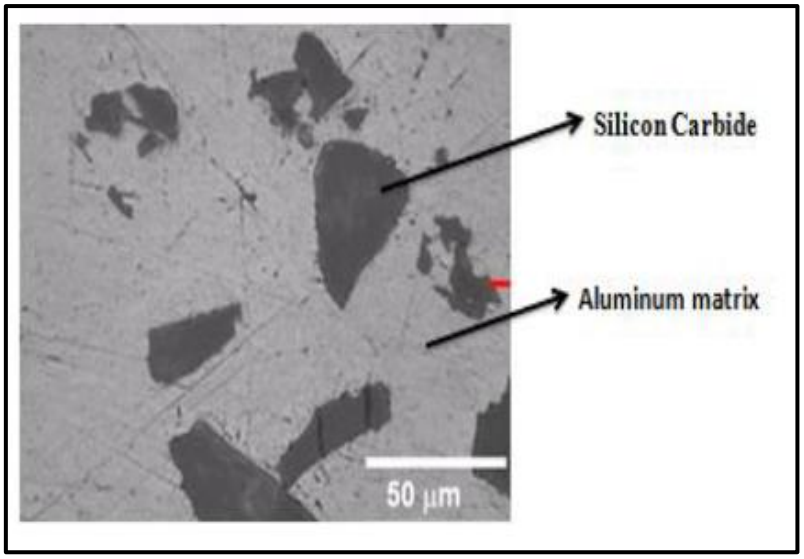

Figure 2.5 Raster image [30].

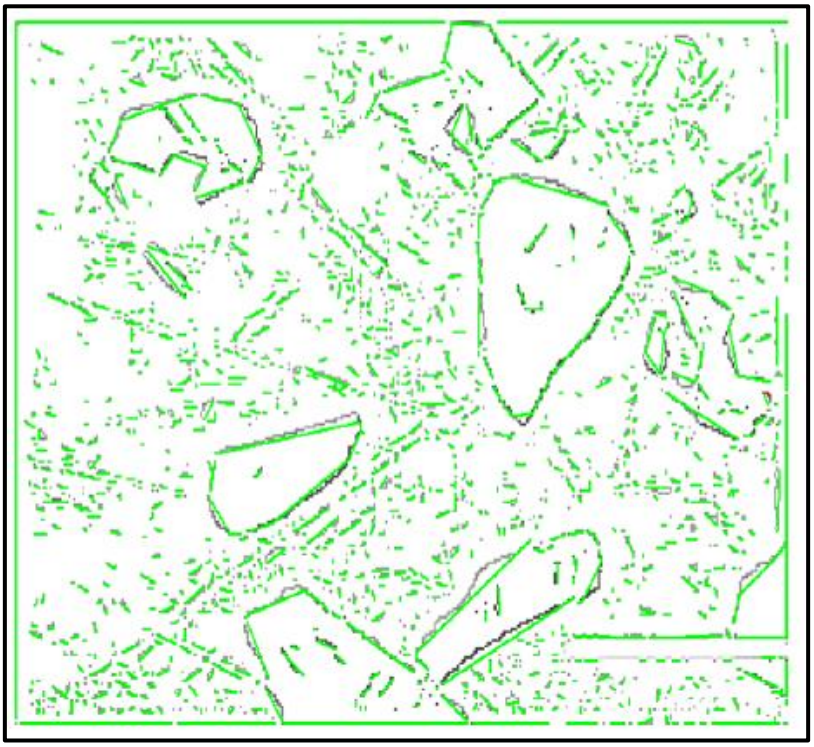

Figure 2.6 Vector image [30].

Vector image of microstructure was now imported to Auto Cad software (via the DXF file format). Figure 2.7 shows that edges of the microstructure were drafted and redundant asperities were removed on importing.

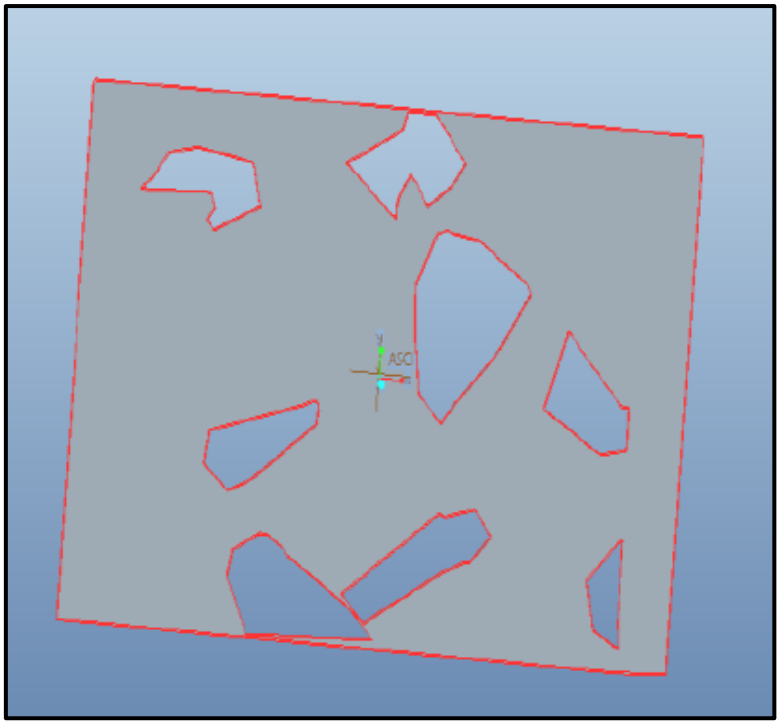

Figure 2.7 Edited image using Auto Cad software [30].

Finally, Hyper Mesh software was used to generate FEM model (235384 nodes; 67348 elements) from the CAD model (see Figure 2.8).

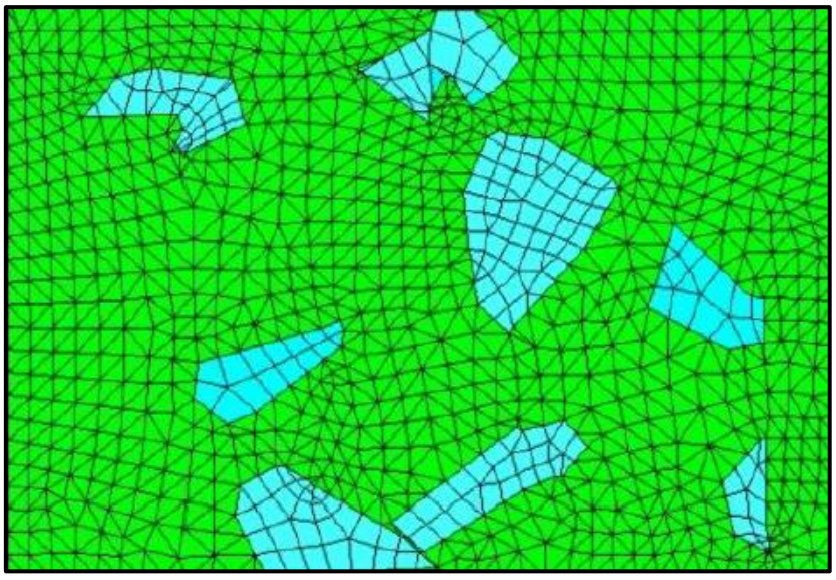

Figure 2.8 Meshed image [30].

Two-dimensional microstructure model meshed properly in Hyper Mesh was imported to Ansys to perform analysis. Young's modulus for aluminium matrix and silicon carbide

particles was 72.5 GPa and 410 GPa respectively. Poisson's ratio for aluminium matrix and silicon carbide particles was 0.33 and 0.19 respectively.

Micro-deformation behaviour of composite microstructure was studied using FEA. Stress distribution pattern (tensile load: 500 N) determined that plastic flow initiated at particle corners (Figure 2.9) and strain along sides of particles (Figure 2.10).

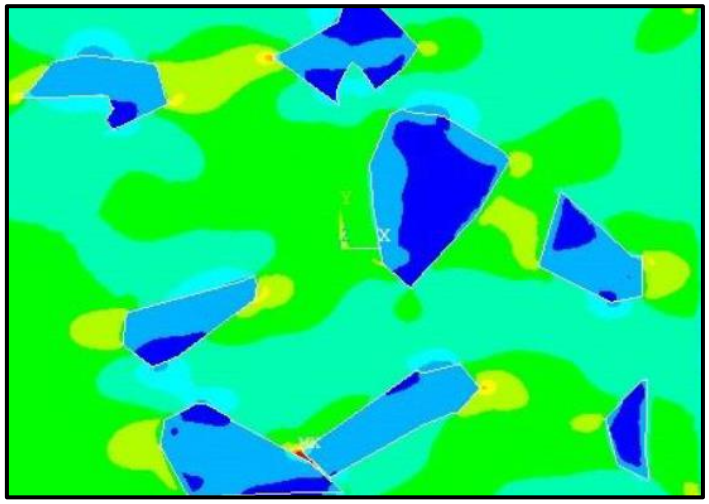

Figure 2.9 Plastic flow in matrix [30].

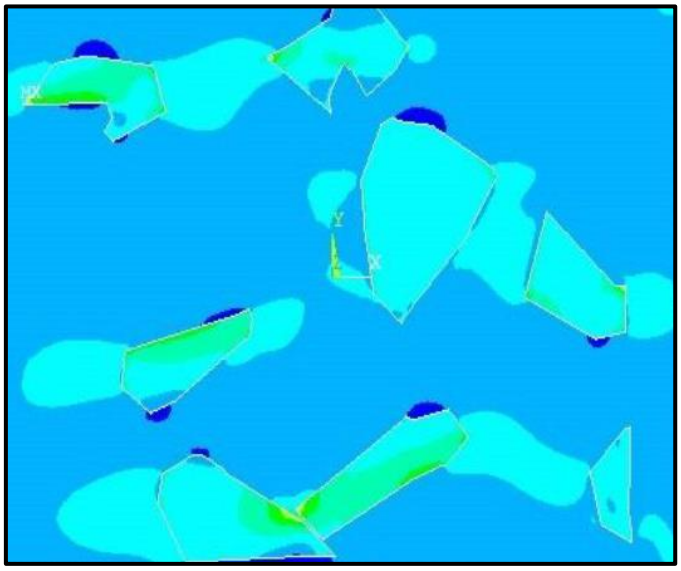

Figure 2.10 Strain distribution in matrix [30].

Stress-strain graph (Figure 2.11) determined the Young's modulus as 82.5 GPa.

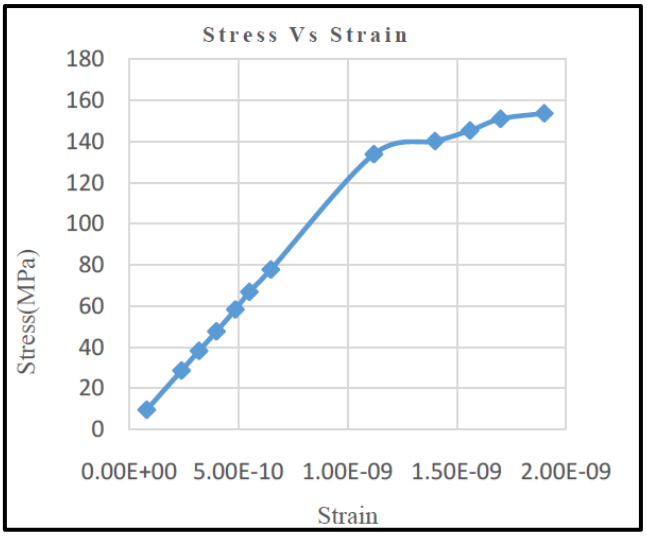

Figure 2.11 Stress-strain graph [30].

Lai *et al.* [31] studied the influence of MVF on fracture behaviour of DP steels. Steel chemistry was 0.1% C and 3.4% Mn (by wt. %). DP microstrucuture was obtained by quenching of hot rolled ingot (900 ℃) which was followed by cold rolling (70% reduction). Subsequentely, tempering was done. Finally, annealing (700 ℃) for duration ranging from 20 min to 6 h. Standard metallographic techniques were used to prepare samples for SEM analysis while quantitative image analysis for calculating phase fraction was done viz Image J. Nano-indentation test were performed to locally probe martensite hardness. Mechanical properties were evaluated with the help of tensile testing machine with standard dog bone samples (gauge length: 25 mm; strain rate: 0.001/s). DP microstructure with 15%, 19%, 28% and 37% MVF were obtained by annealing at 700 ^{o}C for different soaking period. The tensile properties of the different annealing conditions were obtained. It was observed that tensile strength increased with increasing MVF but at the cost of uniform elongation and true strain. This was mostly attributed to the progressive elasto-plastic transititon with higher MVF. The authors also observed that MVF had a significant effect on the fracture behaviour of the observed specimens. It was proposed that fracture in DP steels was either due to interface de-cohesion at ferrite-marteniste boundary or due to micro-crack initiation and growth along the martensite islands. It was reported by the authors that micro-void initiation was followed by interface de-cohesion in case of DP microstructure with lesser MVF. However, martensite fracture leading to micro-void initiation happened with increasing MVF in the steels.

Ohata *et al* [32] developed a meso-scale 3D model similar to the microstructure of dual phase (ferrite-pearlite) steel for analysing stress-strain behaviour of microstructure. Further, a damage evolution model was generated for depicting void growth by simulations using Abaqus

software. Simulation results were compared with experimental results. For modelling, Voronoi tessellation technique was utilized. This technique is transcribed as isotropic crystal growth process. In this, grain growth occurs at the same rate in all directions and growth is terminated for each cell whenever it comes close to a neighbouring cell. The space of target volume (50µm×50µm×50µm) was selected for distribution. Second phase of steel was selected by generation of random numbers. Figure 2.12 depicts the method of creating the dual phase FE model and the complete developed model is depicted in Figure 2.13. Model details include: polycrystalline model, number of grains: 187, pearlite volume fraction: 30%, average grain size: 25 µm.

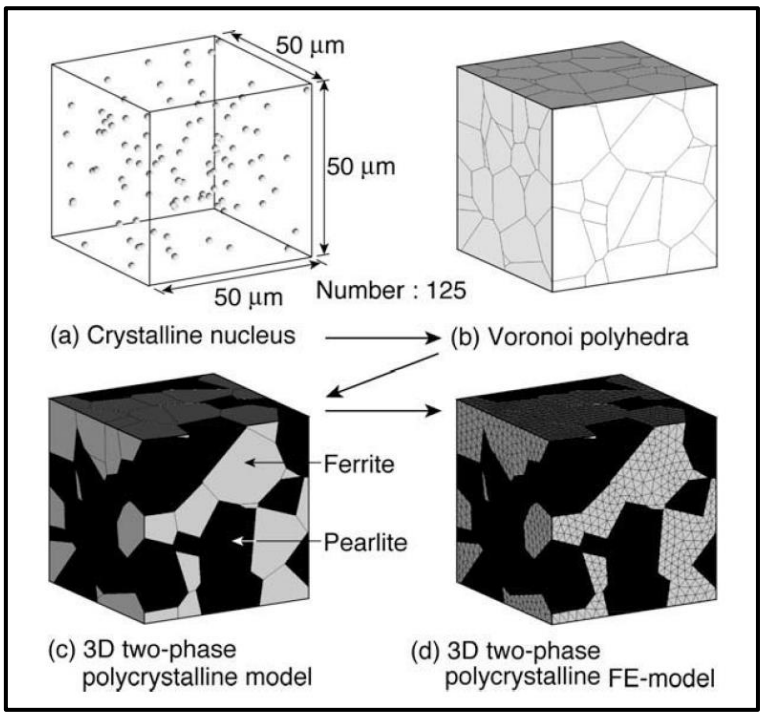

Figure 2.12 Method of creating dual phase FE model [32].

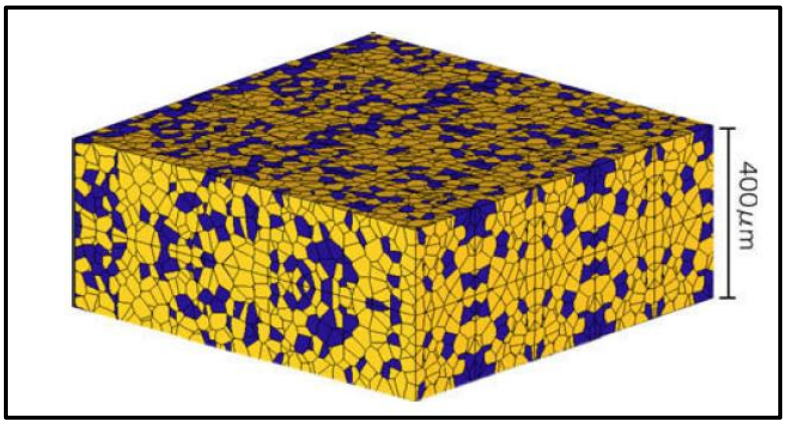

Figure 2.13 Example of dual phase model generated by developed method [32].

After completion of FE-analysis based simulation, it was concluded that experimental results and simulation results were in good agreement. It was concluded that micro-voids originated on the ferrite side in the vicinity of ferrite-pearlite boundary. After the origin of micro-voids, fracture followed.

Singh *et al.* [33] examined influence of martensite morphology/distribution on tensile strength of specimens processed through three main annealing routes.
Table 2.3 presents the steel chemistry.

Table 2.3 Chemical composition of the starting material [33].

Element	C	Mn	P	S	Si	Al	N
(wt. %)	0.074	1.83	0.012	0.002	0.43	0.026	0.0032

The various annealing routes used by the authors to obtain DP microstructures with differences in morphology and distribution of martensite are shown in Figure 2.14.

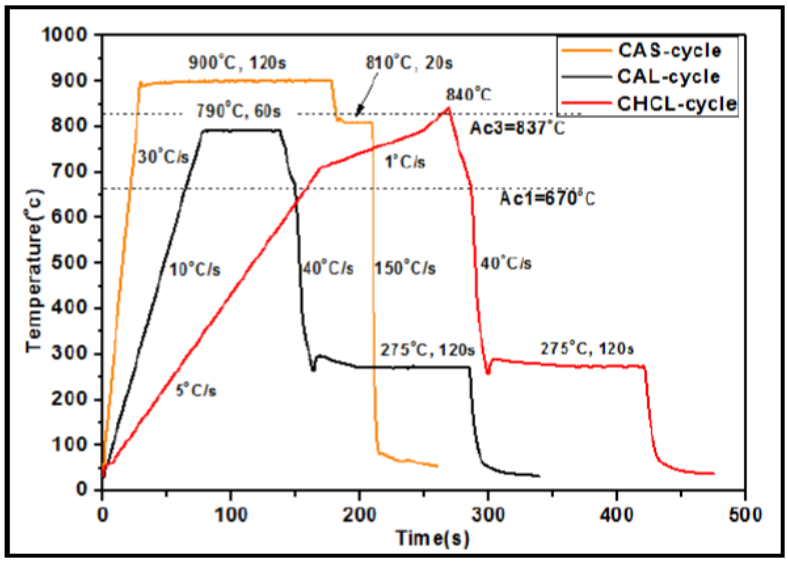

Figure 2.14 Different annealing routes of CAL, CHCL, and CAS used in the research [33].

The annealing route followed for industrial processing of DP steels is the CAL route. The other two routes are modifications over this industrially used process. Continuous annealing line process (CAL route) produced DP microstructure with ferrite as the primary phase (martensite fraction was only 20%) with martensite phase mainly present on the grain boundaries of ferrite. The second annealing process called continuous heating and cooling line (CHCL route) produced DP microstructure with same volume fraction of phases (MVF = 20%) as was produced by the CAL route. The main difference between DP microstructures produced by

CAL and CHCL processes was in martensite distribution. For DP microstructure produced by CHCL route, martensite was present at grain boundaries and also within the ferrite grains (i.e. both grain boundary martensite as well as in-grain martensite were present). The microstructure obtained through 'core and shell' process (CAS route) was quite different. CAS route produced DP microstructure with martensite as the primary phase (martensite fraction was 67%). For this annealing route, a typical core and shell type microstructure was obtained. Martensite was present in the core and was surrounded by ferrite channel network which formed the shell of the microstructure. This type of microstructure (core and shell) is typically referred to as harmonic structure in DP steel literature.

The three main types of DP microstructures obtained in the research work are shown in Figure 2.15.

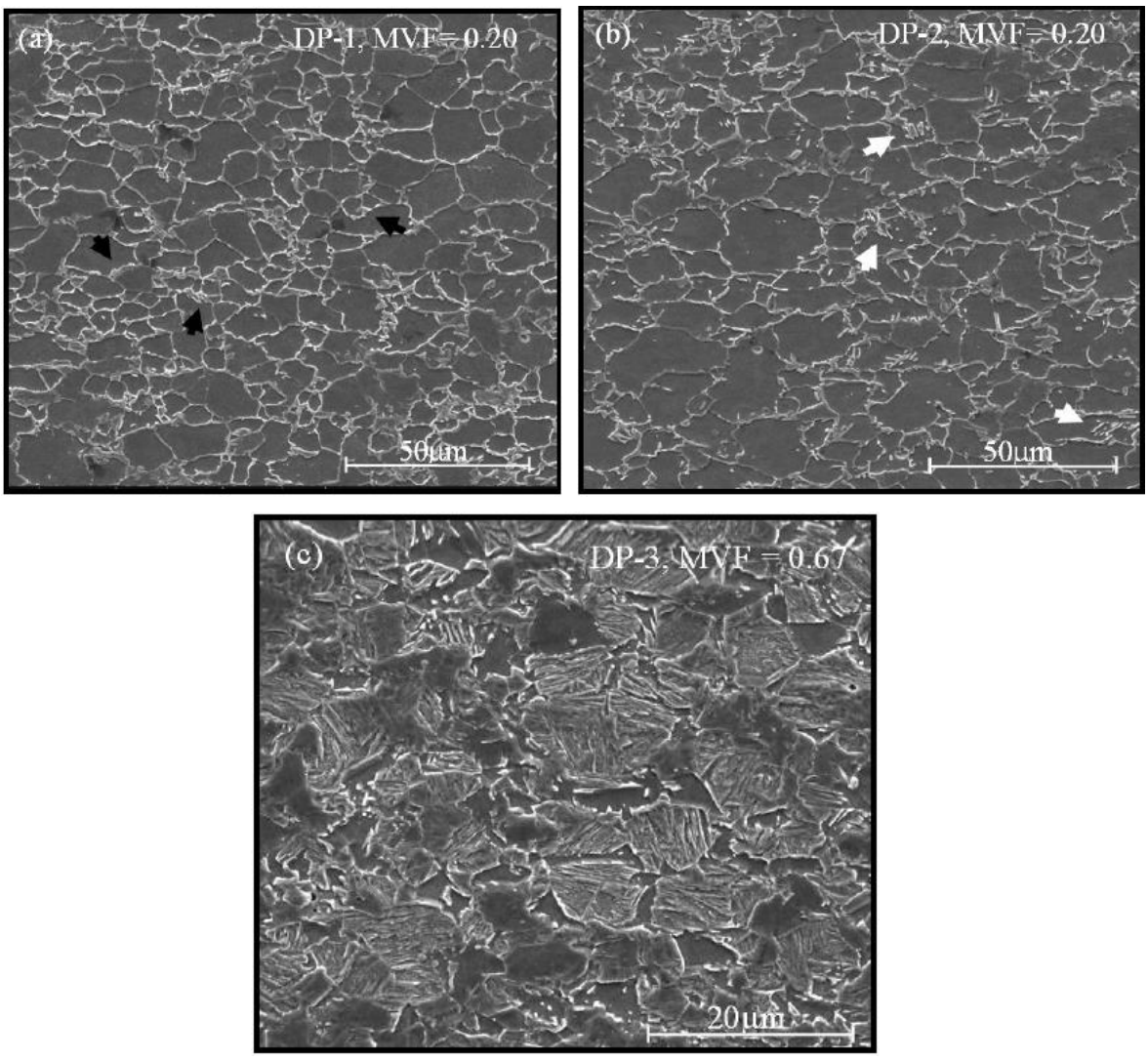

Figure 2.15 SEM micrographs of (a) CAL, (b) CHCL, and (c) CAS processed steels. Black arrows indicate grain boundary martensite and white arrows indicate in-grain martensite [33].

The results of tensile testing are presented in Figure 2.16.

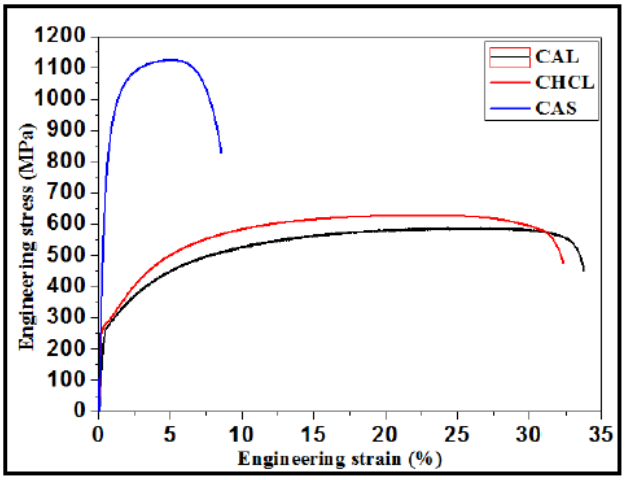

Figure 2.16 Tensile test results for various DP steels [33].

The results showed that CALCHCL routes provided moderate strength-high ductility combination in DP steels. However, deformation behaviour of CAS processed steel was quite different with very high strength but low ductility.

Kumar *et al.* [34] examined the influence of annealing routes on ferrite channel deposition around martensite phase in DP steels.

The composition of the starting material is shown in Table 2.4.

Table 2.4 Steel chemistry of the starting material [34].

C	Mn	P	S	Si	Al	Cr	N
0.091	1.86	0.014	0.007	0.47	0.038	0.017	0.0035

The various annealing routes followed in the research work are shown in Figure 2.17. Three different peak annealing temperatures (PAT) were used to get three different microstructures. The annealing temperatures were 1000 ℃, 1050 ℃, and 1100 ℃ respectively.

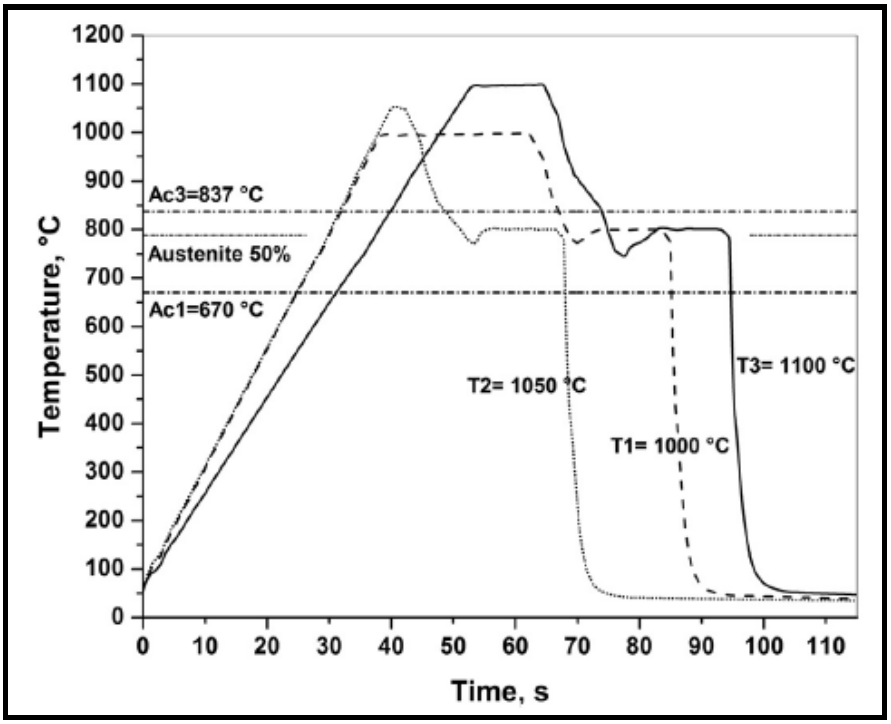

Figure 2.17 Annealing profile used for processing the samples at three different peak temperatures [34].

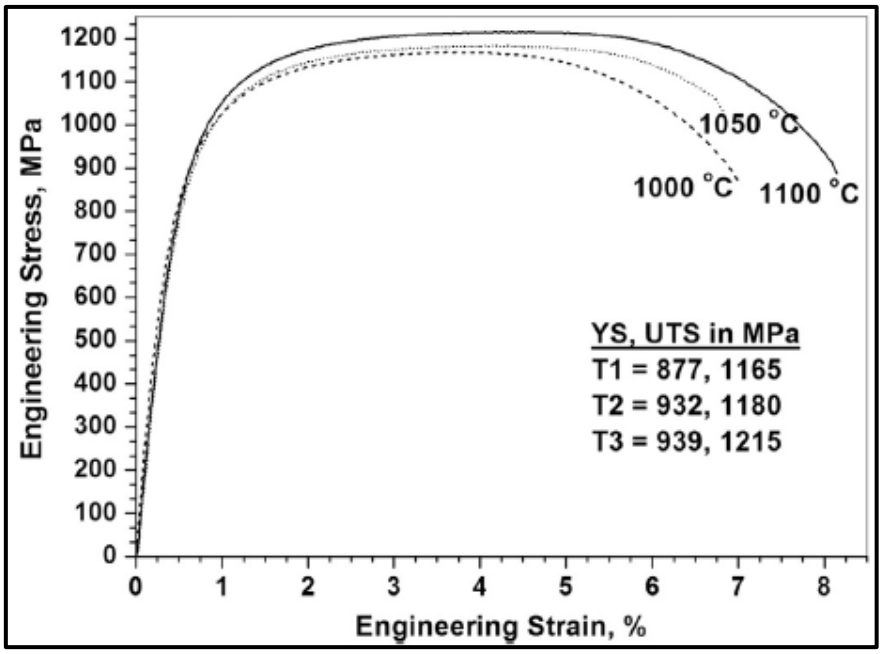

Figure 2.18 Tensile results for three different temperature peaks [34].

The results of tensile testing are presented in Figure 2.18. Core and shell type of microstructure was formed at 1100 ℃ in which soft phase ferrite in the form of a channel network surrounded the martensite phase.

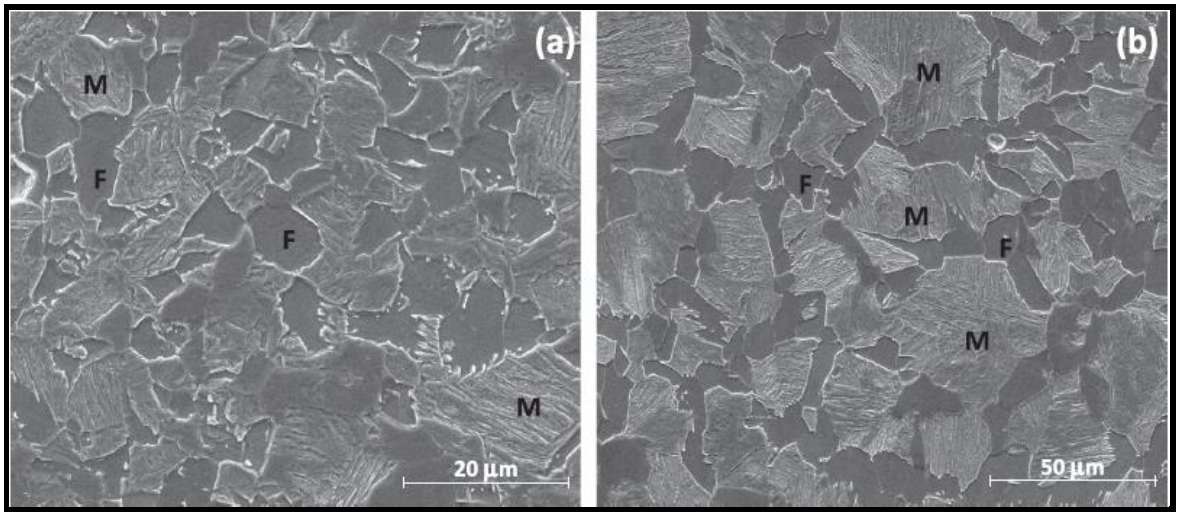

Figure 2.19 Microstructure evolution showing dual phase formation by annealing process at (a) 1000 ℃ and ferrite channel formation at (b) 1100 ℃ [34].

The results of tensile testing showed that the core and shell type DP microstructure produced with peak temperature of 1100 ℃ produced the best mechanical properties. For this harmonic structure, the authors reported that inter-lath martensite crack formation was dampened by ferrite shell surrounding the martensite core.

2.2 Summary of the existing literature

- A few authors have investigated the effect of annealing parameters on the microstructure and tensile properties of DP steels. The authors have varied the heat treatment process parameters to mainly change the martensite volume fraction in the DP microstructure and hence the resultant properties [21, 22, 27, 28]. A few authors have tried and successfully altered the martensite distribution for the same volume fraction of constituent phases in DP microstructure [20, 34]. Also, a few authors have investigated the influence of ferrite grain size on properties [24].
- Saeidia *et al.* [25] developed a new type of DP steel named laminated dual phase (LDP) steel. Two types of steels St37 (middle layer) and IF steels (outer layers) were stacked after surface preparation. Subsequently, a procedure involving cold rolling, austenization, and quenching was performed. It was concluded that by using the new LDP method, the thermo-mechanical treatments could be avoided. With the new LDP method, better control of MVF could be obtained by selecting an appropriate middle layer.
- Some authors have studied the mechanical properties of SUS 329J1 by creating a harmonic structure (a typical DP microstructure) in the given steel compositions. Harmonic

structured materials exhibited remarkable uniform elongation along with significant strengthening [23, 26].

- Few authors have studied the strain partitioning of martensite phase and propagation of micro-voids, both experimentally and through modelling and simulations [29, 32]. Modelling is done numerically and using voronoi tessellation techniques. The simulation results which were in agreement with the experimental results depicted the deformation produced regions and crack originating and propagating areas. Also, Kumar *et al.* [30] converted SEM image directly to the 2-D meshed image and performed the analysis. The simulation results depicted the deformation behavior, stress distribution of composite and obtained stress-strain graph showing results.

2.3 Gaps in the existing literature

- A few authors have investigated the effect of change in microstructure on the mechanical properties of DP steels. However, in most of the studies, either change in volume fraction of martensite and/or change in ferrite grain size has been discussed. There are only a few studies reporting on the effect of morphology and distribution of martensite islands on the tensile deformation behaviour in dual phase steels.
- Most of the literature reported on DP steels has focused mainly on ferrite/martensite microstructure. Very limited literature is available on dual phase steels with ferrite/bainite microstructure. Further, very limited research is reported on DP steels processed through the CAS route to obtain harmonic structured DP steels.
- There is limited literature reporting on modelling of DP microstructures and their subsequent simulation to explain the tensile deformation behaviour. Authors have explained the tensile deformation behaviour and damage mechanisms based on experimental results. Microstructural analysis of fractured surfaces of tensile specimens have been used to explain the deformation behaviour. There is a lack of literature to explain the tensile properties and deformation behaviour of a given DP microstructure through modelling and simulation.

CHAPTER 3
DESIGN OF THE STUDY

3.1 General

After studying the gaps in existing literature, this chapter discusses the formulation of research objective for the dissertation work. The chapter also discusses the details of starting material, the key issues, and the methodology used in the present experimental/simulation work. Further, a brief description of various equipment and software used for dissertation work is presented.

3.2 Establishment of objective function

Literature review revealed that the harmonic structure design (core and shell) is considered as a new generation of microstructural engineering for inducing plasticity in ultrafine-grained materials [35–37]. Harmonic structure comprises of soft coarse-grained region referred to as core, surrounded by hard ultrafine-grained region referred to as the shell. Ultrafine-grained hard shell provides strength and coarse grained soft core imparts good ductility [38–39]. Powder metallurgy is an established processing route for production of harmonic structure in materials. This was well demonstrated for Ti-6Al-4V alloys [40] and stainless-steel alloys [23] to achieve an effective combination of strength and ductility in ultrafine-grained regime.

DP steels consist of martensite phase (hard phase: imparting high strength) and ferrite phase (soft phase: providing elongation). These steels have been widely used in automobile units because of their good mechanical properties providing good strength-ductility combination [17,41–42]. Now-a-days, research has focused on development of DP steels with lean composition [43]. Parallel to this, new processing techniques have also been developed to control the microstructure evolution which improves the strength-ductility combination. Controlled annealing is one of the techniques used to alter the ferrite-martensite morphology of DP steel with lean composition [34]. Mazahari *et al.* [43] developed ultrafine-grained DP steel using different annealing temperature-heating rate combinations and achieved high strength above 1000 MPa with good ductility. Zang *et al*. [44] studied the relationship between martensite fraction and DP steel properties. The authors observed that with increase in volume fraction of martensite, the ductility and strain hardening rate of DP steel decreased. Tasan *et al*. [45] investigated the strain distribution in DP steel during deformation process. The authors found localised in-homogeneous deformation with large strain in ferrite phase compared to martensite phase. Similar results have also been reported by Dan *et al*. [46]. In addition to this,

a few authors have reported the fracture behaviour studies of ferrite-martensite interface debonding and its influence on overall stress-strain behaviour [47–48]. Most of these studies indicate that DP steel properties are dependent on fraction, shape, size, distribution, and morphology of martensite and ferrite. These microstructure-based parameters are accounted for while discussing various strengthening mechanisms of DP steels associated with crack growth activity within the hard martensite phase.

The present dissertation work is an attempt to extend the concept of harmonic structure design on the microstructure of DP steel and to investigate its effect on the strength-ductility combination of the steel. A deviation from the conventional harmonic structure design concept of soft core and hard shell was envisaged in this study. It was proposed to develop a harmonic structure in the DP steel having soft-shell of ferrite phase (three-dimensional network structure) surrounding the hard-core martensite phase. This was a reversal of roles of shell and core compared to those in conventional harmonic structured materials. The resulting microstructure was expected to exhibit different plastic deformation mechanism.

In this present work, five different annealing cycles were used to get distinct DP microstructures having different martensite morphology, distribution, and volume fraction. These five different cycles belonged to two broad annealing categories (i) Continuous Annealing Line (CAL process) and (ii) Core and Shell (CAS process). The CAL process was employed to obtain the conventional DP grade steel 'DP-C' used in industry [49]. Further, the second category of annealing process (CAS) was categorized into four types viz. CAS-1, CAS-2, CAS-3, and CAS-4. CAS processing routes were used to obtain DP microstructures with large volume fraction of martensite and having harmonic (core-shell) microstructure in which martensite grains were surrounded by the channel like network of ferrite. In the present study, the microstructures resulting from CAS-1, CAS-2, CAS-3, and CAS-4 processes were designated as 'HM-1', 'HM-2', 'HM-3', and 'HM-4' respectively.

Thus, the main objective of research was **(i) to develop various dual phase microstructures in the given steel chemistry to evaluate tensile properties, and (ii) to model and simulate the microstructures for investigating the deformation behaviour.**

The key issues to be taken up during the research work were as follows:

(i) To process the as-received samples by different annealing routes (CAL, CAS-1, CAS-2, CAS-3, CAS-4) to achieve DP microstructures having different volume fraction, morphology, and distribution of martensite.

(ii) To obtain the phase fraction of each phase present in the five distinct microstructures using image analysing software 'ImageJ'.

(iii) To evaluate the tensile properties of different DP steel specimens.

(iv) To perform fractographic analysis of tensile specimens to analyse the micro-mechanisms of deformation in harmonic structured specimens.

(v) To generate the DP microstructures using commercial software Dream.3D (microstructures similar to the experimentally developed DP-C and HM-4 structures were generated with help of Dream.3D software).

(vi) To simulate the deformation behaviour of DP-C and HM-4 microstructures using Abaqus software.

(vii) To compare the simulation results with experimental ones with regards to deformation behaviour.

3.3 Experimental procedure

The detailed experimental procedure followed during the research work is described in this section.

3.3.1 Materials and methods

Cold rolled (thickness reduction: 67%; final thickness: 0.83 mm) steel sheet was used as the starting material. Table 3.1 presents the chemical composition of the as-received steel. The present steel chemistry is used for the production of DP600 grade steel using CAL process. The starting material was machined/cut and obtained in the form of tensile specimens.

Table 3.1 Alloy chemistry of the starting material.

Elements	C	Mn	P	S	Si	Al	N
Weight percentage (wt.%)	0.091	1.86	0.014	0.007	0.47	0.038	0.0035

3.3.2 Annealing simulations

The processing routes for the development of conventional DP microstructure and specific harmonic microstructures were selected after a thorough literature review [33–34, 49]. For the study, two main annealing routes, (a) CAL route, and (b) CAS route were selected. Each route provided different morphology, distribution, and volume fraction of martensite in the dual phase microstructure. The first cycle (referred as CAL) was performed as is used in industry [49]. The second cycle (referred here as CAS) was obtained by some modifications to the annealing cycles viz. modifications in heating rates, holding time, and cooling rates [33–34,

49]. The second cycle (CAS) was further sub-divided into four different cycles (CAS-1, CAS-2, CAS-3, and CAS-4). All the annealing cycles were carried out in a hot dip process simulator (HDPS). Table 3.2 presents the various process parameters used for different annealing cycles. These annealing cycles are described in the following sub-sections.

Table 3.2 Annealing process parameters used in the present study [33–34, 49].

Annealing Process	Heating rate to reach Stage-I Temperature.	Stage-I Temperature/ Time	Stage-II Temperature /Time	Stage-III Temperature/Time
CAL	10℃/s	790℃/60s	a) Slow cool to 675 ℃ b) Fast cool (40℃/s) from 675 ℃ to 300 ℃ c) Hold at 275 ℃/120s d) Fast cool to room temperature	---
CAS-1	17℃/s→A_{C1} (675℃) 2.5℃/s →Stage-I	900℃/120s	a) Fast cool to 780℃ b) Hold at 780 ℃/25s	a) Fast heating to 840℃ b) Hold at 840℃/25s c) Ultra-fast cool to room temperature
CAS-2	14℃/s →A_{C1} 2.5℃/s →Stage-I	900℃/120s	a) Fast cool to 800℃ b) Hold at 800℃/25s	a) Fast heating to 840℃ b) Hold at 840℃/25s c) Ultra-fast cool to room temperature
CAS-3	30℃/s →Stage-I	900℃/120s	a) Fast cool to 780℃ b) Hold at 780 ℃/30s c) Fast cool to room temperature	---
CAS-4	30℃/s →Stage-I	900℃/120s	a) Fast cool to 780℃ b) Hold at 780 ℃/30s	a) Fast heating to 840℃ b) Hold at 840℃/30s c) Free cool to 780℃ d) Ultra-fast cool to room temperature

a) CAL cycle

Continuous annealing line (CAL) cycle used in the present work was similar to the conventional annealing route used in the industry [49]. The specimens were heated to a temperature of 790 ℃ with the heating rates of 10 ℃/s followed by isothermal holding of 60 s as shown in Table 3.2. Inter-critical holding was performed to obtain transformation of pearlite for nucleation and grain growth of austenite. After isothermal holding, cooling was performed in three steps.

i. The first cooling was slow cooling from 790 ℃ to 675 ℃. This stage of slow cooling resulted in carbon enrichment of austenite and ferrite transformation.

ii. The second cooling was fast quenching (40 ℃/s) from 675 ℃ to 300 ℃. Fast cooling rate was essential for the transformation of austenite to martensite and to avoid formation of bainite.

iii. Subsequently, the specimen was held at 275 ℃ for 120 s followed by fast cooling till room temperature. This holding time was required for tempering of transformed martensite. Tempering was done to obtain improved ductility and distribution of martensite in DP steel.

b) CAS cycle

As-received steel sheets were taken in the form of standard tensile specimens and were subjected to annealing processes designated as CAS-1, CAS-2, CAS-3, and CAS-4 to obtain harmonic structured DP steel. The detailed parameters of CAS-1, CAS-2, CAS-3, and CAS-4 annealing processes (including CAL process for reference) are described in Table 3.2. Each annealing process was divided into three different process stages; Stage I- peak austenization, Stage II- inter-critical austenite decomposition, and Stage III- re-austenitisation annealing followed by ultra-fast cooling [33–34, 49].

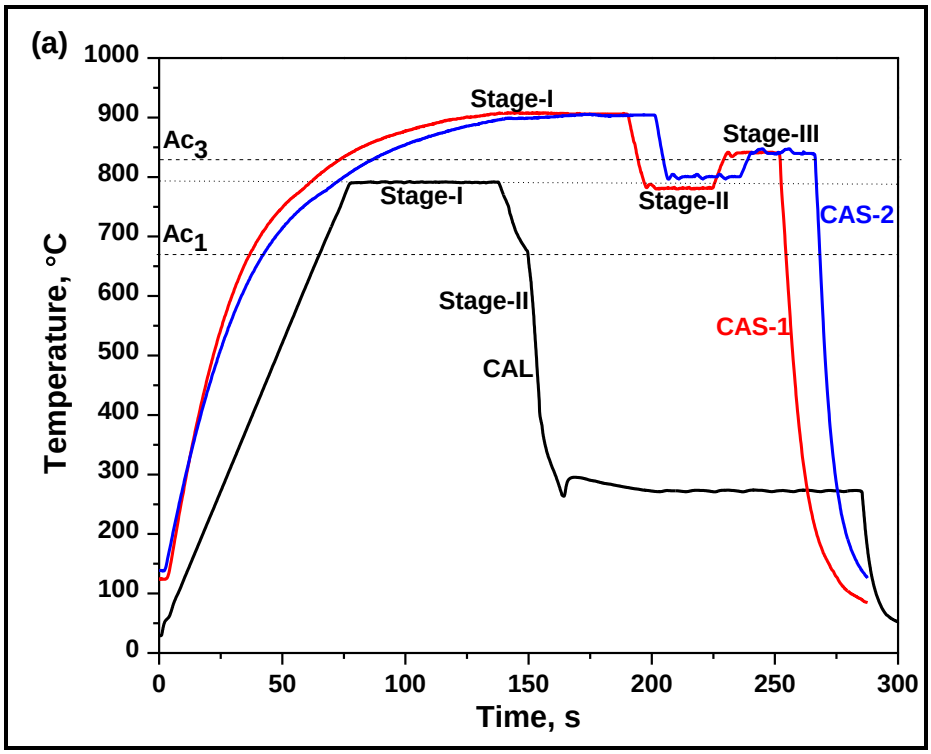

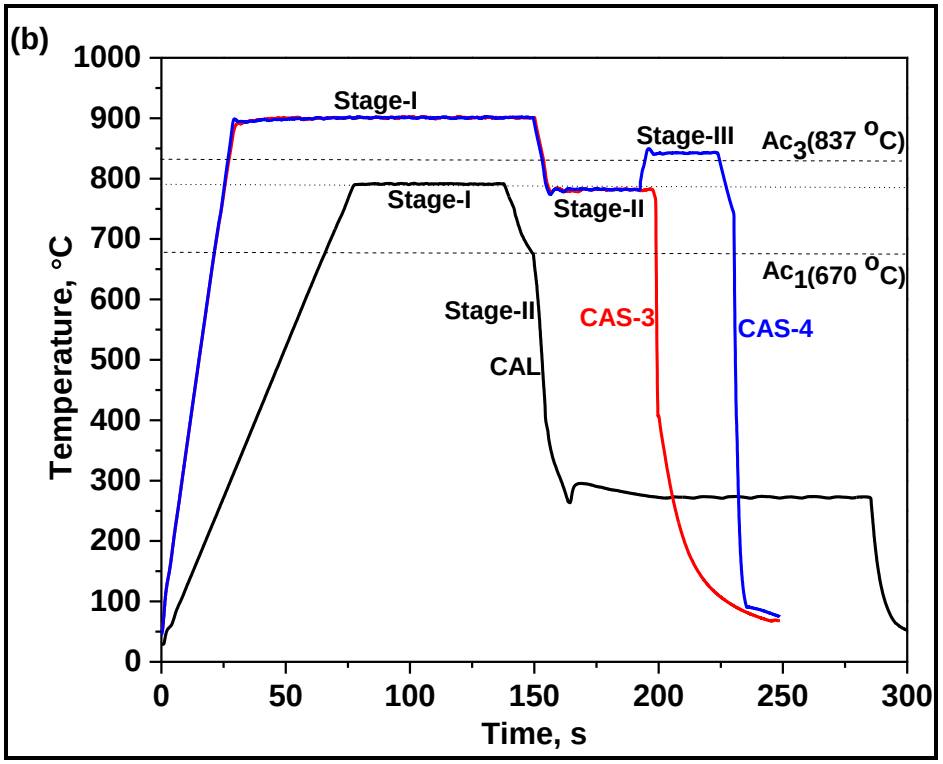

Figure 3.1 Time-temperature profile of various annealing processes (a) CAS-1 and CAS-2, and (b) CAS-3 and CAS-4 along with continuous annealing line (CAL) process for comparison. Ac_1 and Ac_3 temperatures are indicated by dotted lines [33–34, 49].

3.3.3 Microstructure characterization

After annealing, the specimens were prepared for characterization using standard procedure. FE-SEM microscopy (FEI NOVA NANOSEM 430, Field Emission Inc., Hillsboro, USA) was used for the purpose. Quantitative SEM microstructure analysis was carried out to estimate martensite area fraction using image analysis technique. An average of ten microstructure frames were used for the quantitative analysis.

3.3.4 Mechanical property evaluation

Tensile properties of various samples were determined using a tensile testing machine.

3.4 Machines, equipment, and software used

The following section describes the various machines, equipment and software used in the present study.

3.4.1 Hot dip process simulator (HDPS)

HDPS set-up (ICS Iwatani Surtec, Germany) was used for annealing simulations of five different cycles used in this study (see Figure 3.2). Galvanizing and annealing of sheet metal samples can be performed accurately in this highly automated machine. This machine uses

infrared heating system with maximum attainable temperature as 1200 ℃. Heating rates of 30 ℃/s and ultra-fast cooling rates of 150 ℃/s can be obtained. Samples were mounted on the end of a rod which moves in the heating and cooling chamber according to the requirements of the annealing cycle. Thermocouple (k-type) was welded on the sample for obtaining accurate temperature values. To avoid oxidation of steel in the HDPS simulator, a mixture of H_2 (10 %) and N_2 (90 %) was used to create an inert atmosphere. The machine was programmed, and thereafter, the samples automatically moved into the heating and cooling chambers according to the annealing requirements.

Figure 3.2 Hot dip process simulator used (Courtesy: CSIR-NML, Jamshedpur).

3.4.2 Tensile testing machine for testing at quasi-static strain rate

Tensile testing machine (Instron 8501 System, *Instron Engineering Corporation*, Norwood, USA) with a loading capacity of 100 kN (see Figure 3.3) was used for tensile testing (gauge length: 35 mm; cross head displacement speed: 0.27 mm/min; strain rate: 1.3×10^{-4} s^{-1}).

Figure 3.3 Tensile testing machine for testing at quasi-static strain rate (Courtesy: CSIR-NML, Jamshedpur).

3.4.3 Facilities for sample preparation

This section describes the machines and equipment used to prepare samples for metallographic examination.

(a) Precision Cutter

The precision cutter (Micracut 125, *Metkon Instruments Inc.*, Bursa, Turkey) was used to cut small samples from the tensile specimens for microstructural evaluation. Figure 3.4 shows the precision cutter used in the present work.

Figure 3.4 Precision cutter (Courtesy: CSIR-NML, Jamshedpur).

(b) Mounting

Mounting was done for easy handling of samples. Samples were mounted in copper powder at a temperature of 160 $°C$ in the mounting press (Bainmount Metco, *Chennai Metco Pvt. Ltd.*, Chennai, India). Figure 3.5 presents the mounting machine used in the present study.

Figure 3.5 Mounting press (Courtesy: CSIR-NML, Jamshedpur).

(c) Grinding.

Samples were polished using abrasive papers in order of finer grades in the range 80–2000 mesh size for examining them under microscope. Various abrasive papers used are shown in Figure 3.6.

Figure 3.6 Abrasive papers (Courtesy: CSIR-NML, Jamshedpur).

(d) Polishing

After using abrasive papers, the samples were polished on the polishing machine (BANIPOL METCO, Model No: PMV018, *Chennai Metco Pvt. Ltd.*, Chennai, India) as shown in Figure

3.7 to get mirror like smooth surface. Machine is equipped with two polishing wheels covered with cloth (velvet or canvas) to retain the polishing solution such as alumina etc. Before use, the cloth was thoroughly washed with water to remove contaminations, if any, present from the previous experiment.

Figure 3.7 Polishing machine (Courtesy: CSIR-NML, Jamshedpur).

(e) Etching

Etching performs selective chemical attack on heat treated specimens to reveal different phases. Nital (2% nitric acid in ethanol) was used as the etchant in the present work to reveal the microstructure features.

(f) Levelling

For optical characterization, the specimen surface should be properly flat or levelled. For this purpose, levelling press as shown in Figure 3.8 was used in the present work.

Figure 3.8 Levelling press (Courtesy: CSIR-NML, Jamshedpur).

3.4.4 Equipment used for microstructural evaluation

Field emission scanning electron microscope was used for microstructural characterization in the present work and is described as follows.

a) **Field Emission Scanning Electron Microscope (FE-SEM)**

In the present research, FE-SEM microscope (FEI Nova Nano SEM 430, Field Emission Inc., Hillsboro, USA) captured the micrographs. Quantitative SEM microstructure analysis was carried out for estimating martensite area fraction using image analysis technique. Figure 3.9 shows the FE-SEM set-up used in the present study.

Figure 3.9 Field emission scanning electron microscope (Courtesy: CSIR-NML, Jamshedpur).

3.4.5 Commercial software

In the present study, various software viz. ImageJ, Dream.3D, and Abaqus were used. The details of various software are presented below.

(a) ImageJ

ImageJ (developed by *NIMH*, Maryland, USA) is an open source Java image processing program. This software can analyse and edit various images. The software supports following formats including TIFF, GIF, JPEG, BMP etc. In the present study, this software was used for determining phase fraction and also grain size of martensite phase present in various dual phase microstructures developed in the present work.

(b) Dream.3D

Dream.3D (developed by *Blue Quartz Software LLC*, Springbora, USA) is an open source software for reconstructing, visualizing, and analysing multi-dimensional data. There are various filters available in the software tool box. By using the combinations of various filters, a generic pipeline model can be generated. Essential information like shape and size of martensite and ferrite phases, distance between neighbouring secondary phase constituents, proportion of secondary phase present on grain boundaries etc. were fed to the 'Stats Generator' filter. After generating the pipeline, the data was saved in XDMF file format. Figure 3.10 presents the screenshot of input parameters for modelling the microstructure in Dream.3D software. Figure 3.11 presents the output of Dream.3D software observed using Para View software.

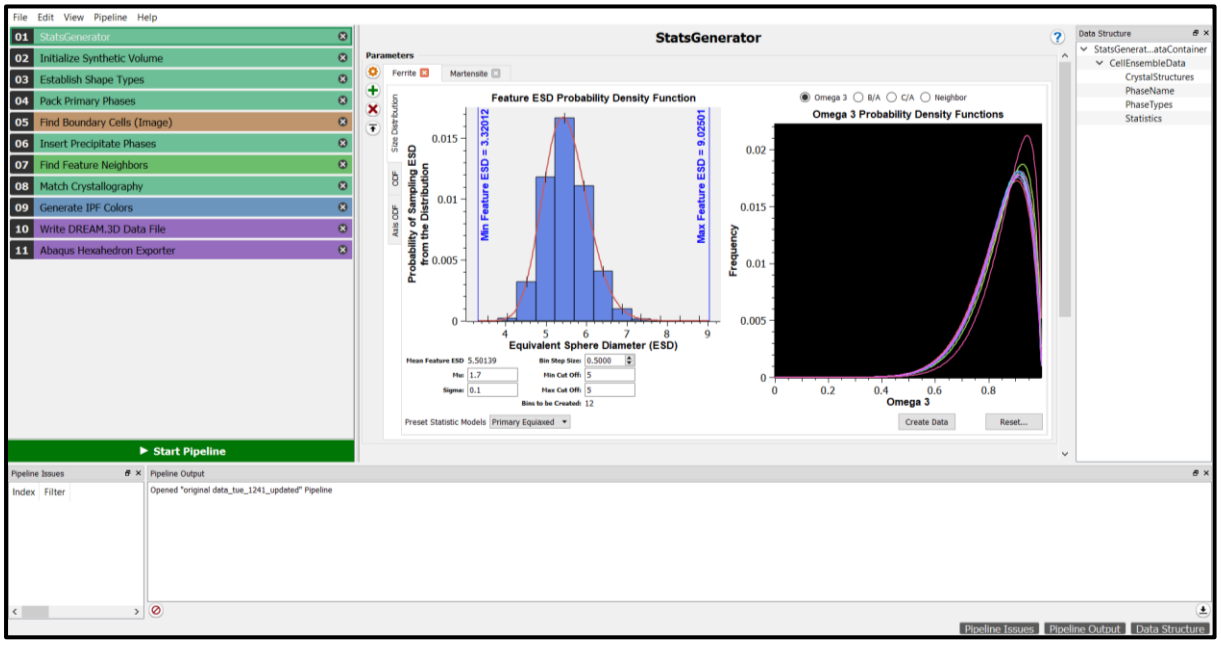

Figure 3.10 Screenshot of input parameters used for modelling of microstructure in Dream.3D software.

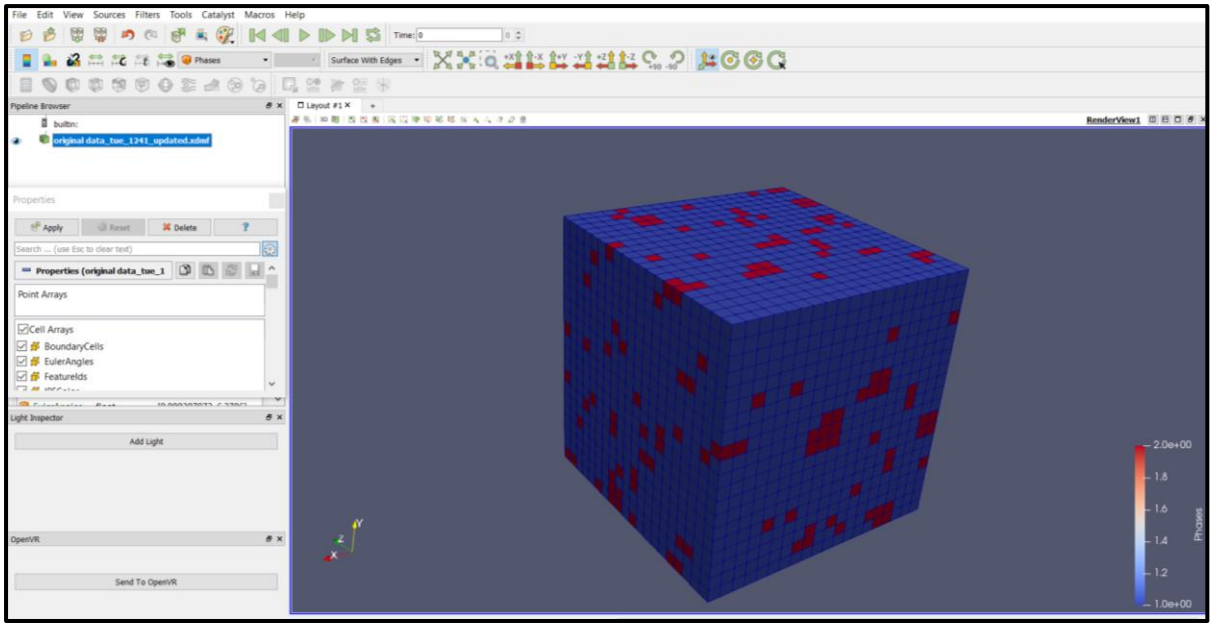

Figure 3.11 Screenshot of Para View software depicting the output of Dream.3D software.

(c) Abaqus

Abaqus (Dassault Systemes Simulia Corporation, USA) is a licenced software. Abaqus/CAE is divided into different modules. Various parameters like geometry, materials properties, and mesh size are defined. Model is developed by using various modules. After development of model, Abaqus/CAE generates the input file. This input file is read by Abaqus/Explicit (or Abaqus/Standard) which performs the analysis. It sends the information to Abaqus/CAE which develops the output database. Finally, a visualization module is used to display the results of analysis. In the present study, the microstructure generated through Dream.3D was imported into Abaqus, where properties of material along with nature of boundary conditions were defined, and finally the required results were obtained.

The detailed procedure for Abaqus software is described as follows:

1. The output file of Dream.3D software available in .inp format could directly be imported and used as an input model for Abaqus software.
2. Next, the materials properties were defined in the property module. For this, two materials (here, phases) namely ferrite and martensite were defined. Further, the elastic properties (Young's modulus and Poisson's ratio) and plastic properties (yield stress and plastic strain) for ferrite and martensite were defined under mechanical drop-down option.
3. Further, the step size of simulation and the outputs (stress and strain) required were defined.
4. Next, in the load module, the boundary conditions including the value of load to be applied were defined. Here the tensile load of 10,000 N was applied (-5000 N in positive X-axis

direction and -5000 N in negative X-axis direction (negative sign indicated the tensile nature of load).

5. Finally, the job was created in the job module where all the above inputs were submitted and the simulation was executed.

3.5 Summary of the chapter

This chapter described the design of the study and experimental procedure followed in the present work. This chapter also discussed the objective and key issues of the present research. Finally, an overview of various machines, equipment, and software used to achieve the above tasks were discussed.

CHAPTER 4

RESULTS AND DISCUSSION

4.1 General

This chapter discusses the various results observed in the present research work. The annealing cycles were performed on the specimens. After annealing, tensile properties were determined. Samples were subjected to SEM microscopy to obtain microstructure related details. Simulation results with regards to the deformation behaviour (developed using Dream.3D and Abaqus software) were compared with the experimental results of actual tensile tests.

4.2 Microstructures obtained through various annealing cycles

The details of different DP microstructures obtained through various annealing routes are presented in this section.

4.2.1 CAL process

SEM micrograph of CAL processed specimen is shown in Figure 4.1. A typical DP microstructure was obtained with martensite volume fraction (MVF) as 22% (obtained using ImageJ). Martensite phase was largely present as grain boundary martensite at the grain boundaries of ferrite phase. The microstructure obtained by CAL process is a typical microstructure of DP600 steel. In SEM image, greyish-black region represents ferrite phase and white region represents martensite phase.

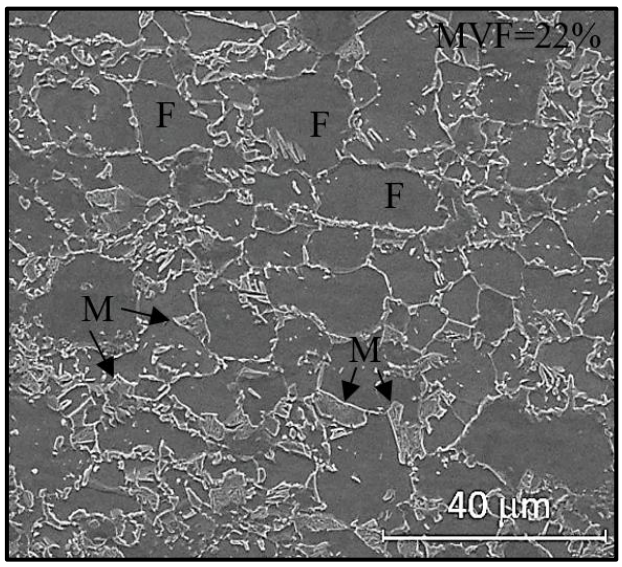

Figure 4.1 SEM micrograph of DP steel processed by CAL route. F= ferrite, M= martensite (mainly present at grain boundaries of ferrite).

4.2.2 CAS processes (evolution of harmonic structure)

The detailed microstructure examination is presented as follows.

a. CAS-1 annealing process

Figure 4.2 presents the microstructure of specimen processed by CAS-1 annealing process. Presence of dual phase microstructure was observed, and it was designated as HM-1. Figure 4.2a–b shows that in the dual phase HM-1 microstructure, martensite phase (core) was surrounded by ferrite phase network (shell).

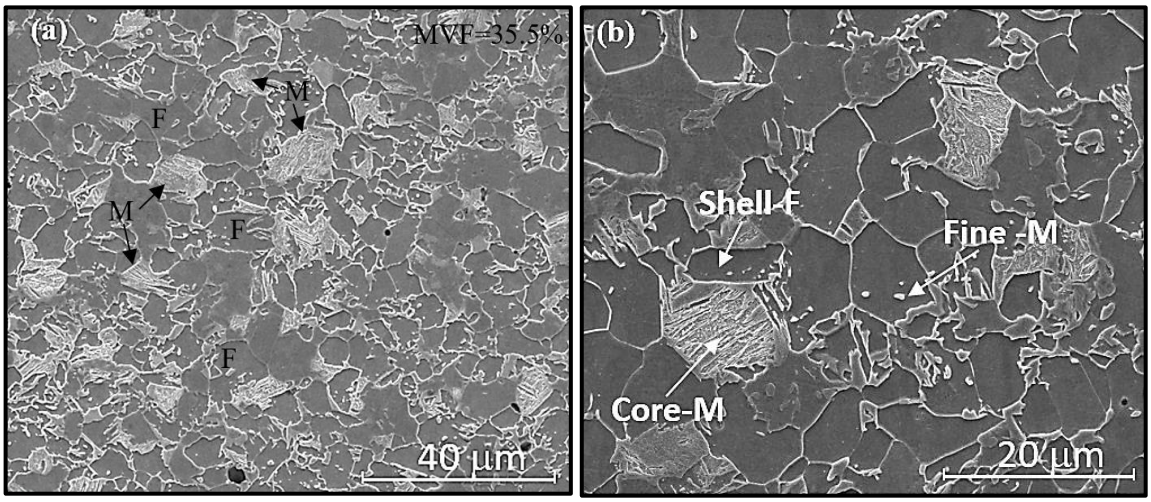

Figure 4.2 SEM micrographs of core-shell harmonic structure of CAS-1 specimen consisting of scattered M-martensite core surrounded by F-ferrite shell network having fine secondary martensite within shell, shown at (a) lower magnification, and (b) higher magnification.

The volume fraction, size, and distribution of martensite phase strongly depend on the annealing process parameters at all three annealing stages (Stage-I, Stage-II, and Stage-III; see Figure 3.1). During Stage-I, the cold rolled steel was subjected to austenization temperature of 900 ℃ (above A_{C3}), to obtain full austenite phase. Austenite phase produced by Stage-I was used for microstructure tailoring to develop harmonic structure in the subsequent annealing at Stage-II and Stage-III. In Stage-II, fully austenitic steel was fast cooled to an inter-critical annealing temperature of 780 ℃, and was held here for a short period (25 s). The Stage-II of annealing process was to trigger controlled decomposition of austenite by nucleation of ferrite along its grain boundaries to form a ferrite network. In Stage-III, this dual phase microstructure (austenite + ferrite network) was rapidly heated to 840 ℃ (above A_{C3} temperature) for partial re-transformation of newly formed ferrite network into fine secondary austenite phase [34]. Thus, at the end of Stage-III, the

microstructure constituted of primary austenite surrounded by ferrite network having secondary austenite within the network. Finally, the steel was ultra-fast cooled (cooling rate of~150 ℃/s) to completely transform primary and secondary austenite into martensite. The resulting DP microstructure consisted of martensite core and ferrite shell (see Figure 4.2).

b. CAS-2 annealing process

Figure 4.3 presents the dual phase microstructure of specimen evolved by CAS-2 annealing route. This DP microstructure was designated as HM-2 and its MVF was 43.5%. The spacing between two martensite cores in the harmonic structure was less as compared to HM-1 steel. Concurrently, refinement of ferrite grain size distribution was noticed. Further, fraction of dispersed fine secondary martensite was increased within the ferrite shell network.

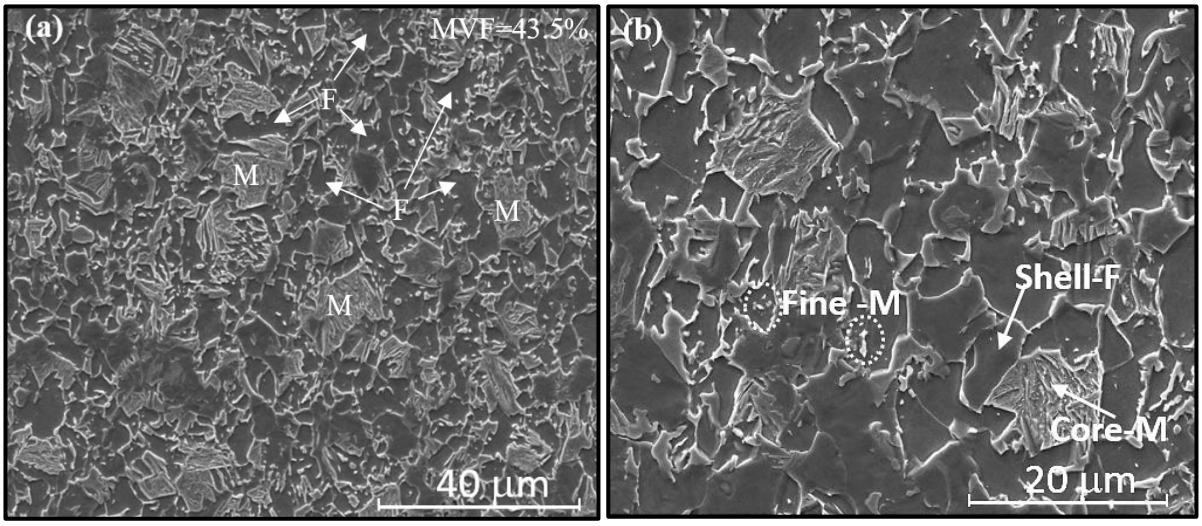

Figure 4.3 SEM micrographs of core-shell harmonic structure of CAS-2 specimen consisting of scattered M-martensite core surrounded by F-ferrite shell network having fine secondary martensite within shell, shown at (a) lower magnification, and (b) higher magnification.

These differences in the microstructures of HM-1 and HM-2 steels were primarily due to variations in the annealing process parameters of Stage-II (of CAS-1 and CAS-2 processes). The inter-critical isothermal annealing temperature was set at a relatively higher temperature of 800 ℃. Annealing at higher temperature increased the stability of austenite during Stage-II, which in turn, made more austenite grain boundary area available for ferrite network formation during this stage. The increase in ferrite nucleation sites resulted in refinement of ferrite network. During Stage-III process, this fine ferrite structure promoted formation of fine secondary austenite, which resulted in increased fraction of fine secondary martensite in HM-2 microstructure (Figure 4.3b).

c. CAS-3 annealing process

Figure 4.4 presents the dual phase microstructure evolved by CAS-3 annealing route. This DP microstructure was designated as HM-3 and its MVF was 52.3%. A more distinct evolution of harmonic structure of core and shell type morphology was observed. This was again made possible by modifying annealing process parameters. Initial heating rate was higher (30 ℃/s) to reach Stage-I (900 ℃) as compared to previous routes. This initial higher heating rate (30 ℃/s)) reduced the austenite grain size at the end of Stage-I of CAS-3 route which led to an increase in austenite grain boundary area for ferrite shell network nucleation in subsequent Stage-II. Further, Stage-III was eliminated (in CAS-3) to avoid formation of fine secondary martensite within the ferrite shell. These fine microstructure details are more discernible at high magnification SEM micrograph (Figure 4.4b). MVF for HM-3 was above 50% indicating transition from pre-dominant ferrite-based DP microstructure to martensite-based DP microstructure. Though this fraction of martensite in DP-3 (MVF = 52.3%) was higher than at in HM-2 (MVF = 43.5%), it was mostly in the form of core of harmonic structure of HM-3 steel.

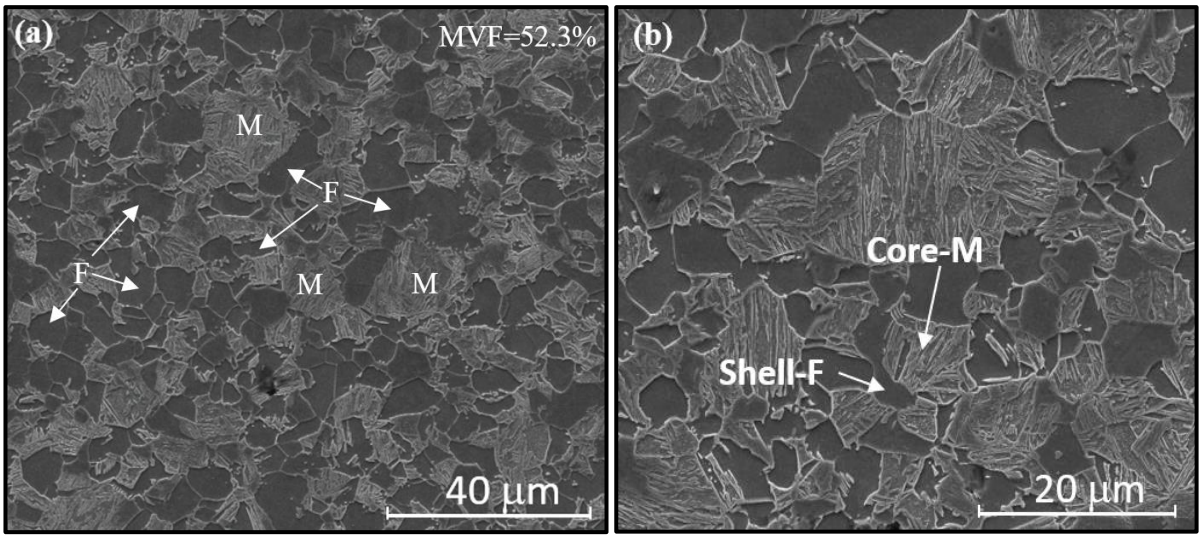

Figure 4.4 SEM micrographs of core-shell harmonic structure of CAS-3 specimen consisting of scattered M-martensite core surrounded by F-ferrite shell network, shown at (a) lower magnification, and (b) at higher magnification. Absence of fine secondary martensite within ferrite shell may be noted.

d. CAS-4 annealing process

Figure 4.5 presents the dual phase microstructure evolved by CAS-4 annealing route. This DP microstructure was designated as HM-4 and its MVF was 62.2%. Core size distribution seemed to be very fine in HM-4 steel as compared to HM-3 steel. The first two annealing

stages in CAS-4 process were identical to those in CAS-3 but processing in Stage-III (re-austenization) was introduced in CAS-4.

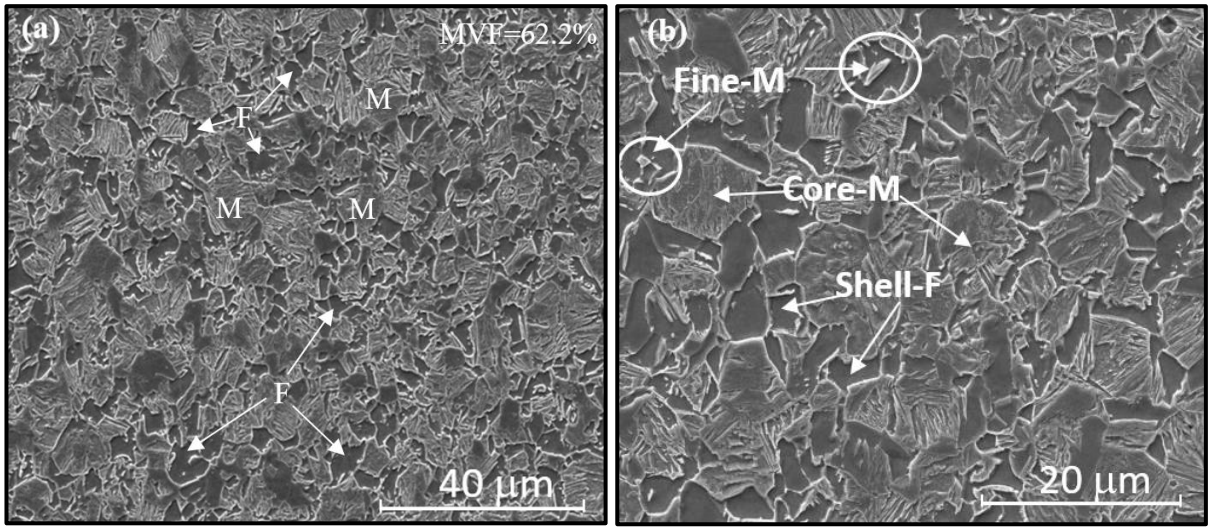

Figure 4.5 SEM micrographs of core-shell harmonic structure of CAS-4 specimen consisting of scattered M-martensite core surrounded by F-ferrite shell network having fine secondary martensite within shell, shown at (a) lower magnification, and (b) higher magnification.

During Stage-III of CAS-4, partially re-austenized ferrite network at 840 ℃ was cooled back to inter-critical annealing temperature of 780 ℃, and then ultra-fast cooled to room temperature for martensitic transformation. Isothermal re-austenization time used in Stage-III 30 s, which was slightly longer than that of CAS-1 and CAS-2 (25 s). This was done to increase secondary austenite fraction within the ferrite network. Cooling to 780 ℃ was performed to partially re-transform the secondary austenite to fine ferrite. Modification to Stage-III of CAS-4 annealing process helped in introducing secondary fine lath and globular martensite in ferrite shell network (see Figure 4.5b).

4.3 Tensile deformation behavior

The engineering stress-strain curves of different DP steels processed through CAL and various CAS routes are presented in Figure 4.6. Table 4.1 presents the mechanical properties of various steels. Harmonic structured DP steels illustrated continuous yielding behaviour similar to that of typical characteristics of DP600 steel produced by CAL process (see Figure 4.6).

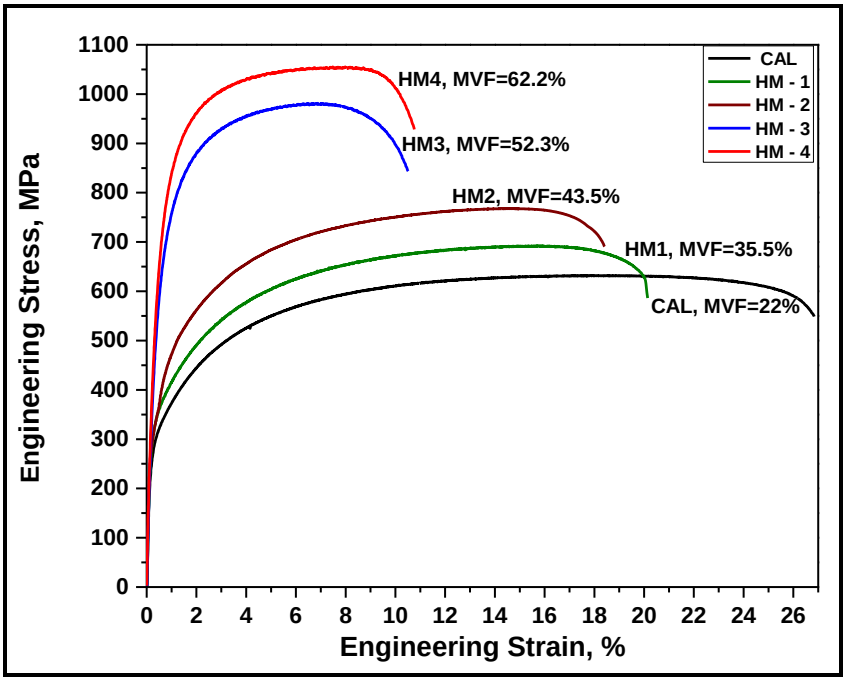

Figure 4.6 Engineering stress-strain curves of various harmonic structured DP steels, along with CAL processed DP-C steel for comparison.

Tensile strength of harmonic structured DP steels (HM-1, HM-2, HM-3 and HM-4) increased whereas ductility decreased with increase in martensite fraction in microstructure.

Table 4.1 Mechanical properties of various harmonic structured DP steels, along with CAL processed DP-C steel for comparison.

Annealing cycle (resulting DP steel)	Martensite volume fraction (MVF), %	Yields strength (YS), MPa	Ultimate tensile strength (UTS), MPa	Uniform elongation (UE), %	Total elongation (TE), %
CAL (DP-C)	22.0	292	631	22	28
CAS-1 (HM-1)	35.5	335	691	16	20
CAS-2 (HM-2)	43.5	362	767	15	18
CAS-3 (HM-3)	52.3	570	980	7.4	11
CAS-4 (HM-4)	62.2	637	1054	8.43	12

This trend (of increased strength/decreased ductility with increased MVF) observed for harmonic structured DP steels in the present study was similar to previous research reported by Zang *et al.* [14]. Noteworthy here is a distinct jump in tensile properties with change in the core-shell morphology (HM-2→HM-3), though the increase in martensite fraction between them was small (~ 9%). Further, between HM-3 and HM-4, an anomalous increase in ductility was observed for HM-4 containing higher martensite fraction (62.2 %) compared to that for HM-3 (52.3 %). A possible explanation for the anomalous behaviour between HM-3 and HM-4 could be due to further refinement in harmonic structure morphology in HM-4. Also, precipitation strengthening effect of ferrite shell network by

fine secondary martensite need to be taken into consideration for the observed high strength in HM-4 compared to HM-3. Probably fine ferrite shell contributed to the overall strength of HM-4 without causing any significant loss of ductility. Therefore, morphology of harmonic structure is also important in DP steel in determining its tensile properties.

4.4 Fracture analysis

SEM micrographs of the fractured tip and area adjacent to it for the tensile tested specimens of harmonic structured DP steels are presented in Figure 4.7a–h. For HM-1 (Figure 4.7a–b) and HM2 (Figure 4.7c–d) steels, micro-cracks/voids mainly originated at (i) ferrite-martensite interfaces, and (ii) secondary in-grain martensite within ferrite grains. Interestingly, the core of the harmonic structure (primary martensite) did not exhibit any tendency of micro-cracking. Further, HM-3 (Figure 4.7e–f) and HM-4 steels (Figure 4.7g–h), consisting of more prominent core/shell type harmonic microstructure displayed very limited martensite micro-cracking tendency in tensile necking zone. Both, core (primary martensite region) and shell (ferrite region) of the DP microstructure showed extensive plastic deformation or plastic strain compatibility. Therefore, even with large fraction of martensite in these microstructures (DP-3/DP-4), the onset of damage activity at ferrite-martensite interface was delayed and that at martensite inter-lath was avoided. Further, damage activity was observed to be mostly restricted at shell/core interfaces (ferrite-martensite interfaces). Thus, the results of present study indicate that local micro-crack propagation or growth rate can be retarded by controlling martensite morphology, wherein martensite as hard core is surrounded by soft ferrite network shell in harmonic structured DP microstructure. Further, ferrite-martensite interface strengthening was achieved by improved plastic strain compatibility of core and shell. This was very much evident from the microstructures as shown in Figure 4.7, illustrating extensive plastic deformation of hard core martensite in the necking region.

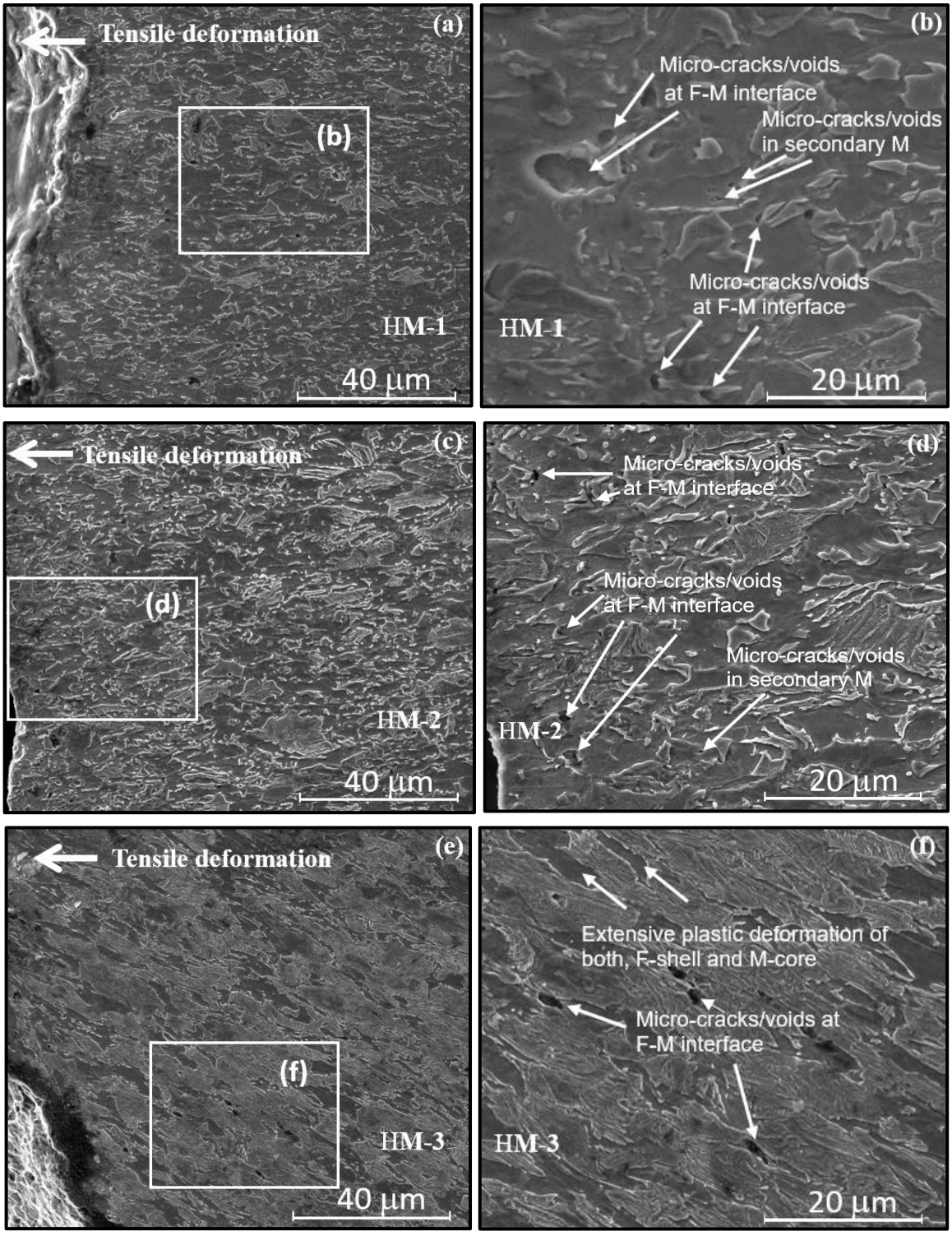
Tensile deformation
(a)
(b)
HM-1
40 µm
(b)
Micro-cracks/voids at F-M interface
Micro-cracks/voids in secondary M
Micro-cracks/voids at F-M interface
HM-1
20 µm
Tensile deformation
(c)
(d)
HM-2
40 µm
(d)
Micro-cracks/voids at F-M interface
Micro-cracks/voids at F-M interface
Micro-cracks/voids in secondary M
HM-2
20 µm
Tensile deformation
(e)
(f)
HM-3
40 µm
(f)
Extensive plastic deformation of both, F-shell and M-core
Micro-cracks/voids at F-M interface
HM-3
20 µm

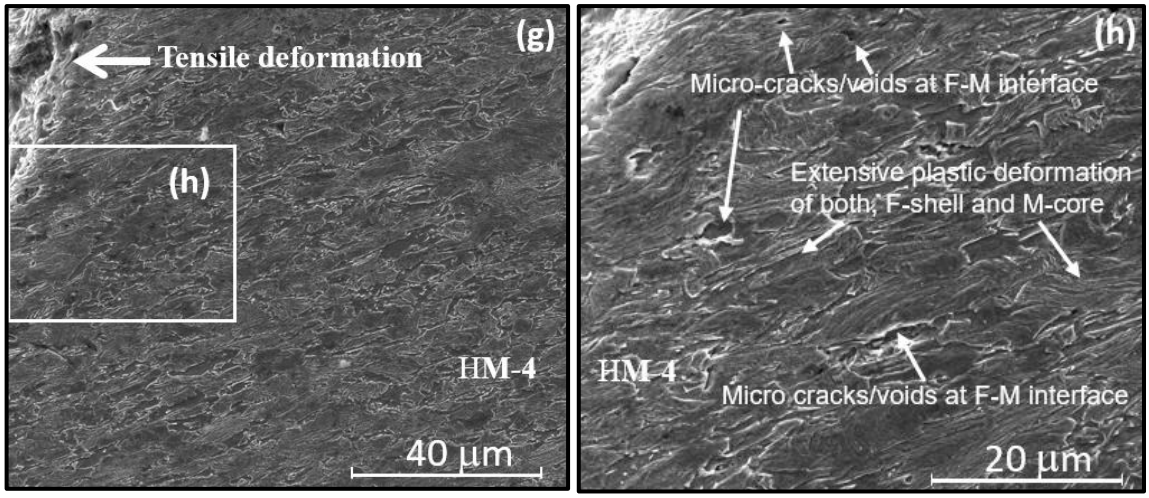

Figure 4.7 SEM micrographs near the fracture end of (a–b) HM-1, (c–d) HM-2, (e–f) HM-3, and (g–h) HM-4 steel specimens showing various damage activities indicated by arrows in (b), (d), (f), and (h) at higher magnification. Extensive plastic deformation of hard core martensite and micro-crack initiation at F-shell/M-core interfaces can be clearly observed in (f) and (h).

4.5 Simulation studies

To investigate the deformation behaviour further, simulation studies were conducted. For simulation work, two main microstructures viz. DP-C (processed through CAL) and HM-4 (processed through CAS-4) were selected. Microstructures similar to DP-C and HM-4 were simulated, modelled, and analysed.

4.5.1 Dream.3D modelling results

Dream.3D software was used to model the microstructures obtained through CAL and CAS-4 processes. In the experimental work, MVF observed for CAL and CAS-4 processes was 22% and 62.2% respectively. In the simulation work, the microstructures developed using Dream.3D for these processes contained similar MVF of 20% (for CAL) and 62% (for CAS-4) respectively. Figure 4.8 presents the Dream.3D output showing microstructures generated by the software. The blue colour in Figure 4.8 represents the predominant phase. It may be noted that the predominant phase for Figure 4.8a (DP-C steel processed by CAL route) is ferrite and that for Figure 4.8b (HM-4 steel processed by CAS-4 route) is martensite.

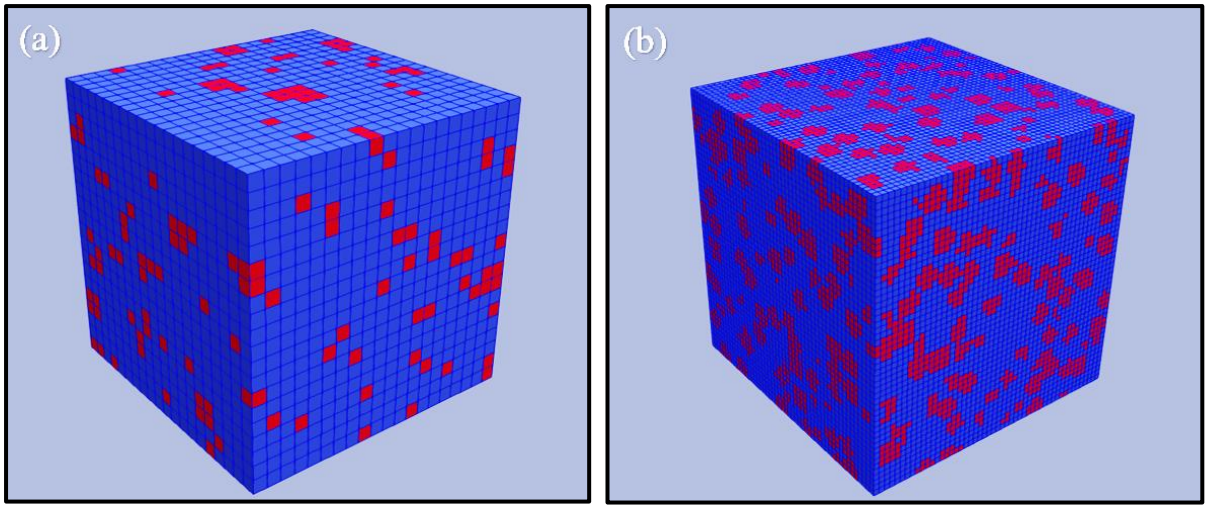

Figure 4.8 Output of Dream.3d software showing representative microstructures generated with (a) 20% MVF (signifying DP-C steel), and (b) 62% MVF (signifying HM-4 steel).

4.5.2 Abaqus simulation results

The output of Dream.3D software was imported to Abaqus software. The stress (S, Mises) and equivalent plastic strain (PEEQ) distribution for microstructures were simulated. The input parameters defining the ferrite and martensite phases are presented in Table 4.2. The initial plastic strain input is zero, by default. To obtain the true stress and true strain values of constituent phases, the values of engineering stress and engineering strain were obtained from tensile curves shown in Figure 4.6. It may be noted that the tensile curve of CAL processed steel with MVF of just 22 % represents a ferrite dominant steel. Hence, the engineering stress and engineering strain values from the tensile curve of CAL processed steel (i.e. DP-C steel) were used to calculate the true stress and true strain values for ferrite phase. Further, the tensile curve of CAS-4 processed steel with MVF of over 62 % represents a martensite dominant steel. Hence, the engineering stress and engineering strain values from the tensile curve of CAS-4 processed steel (i.e. HM-4 steel) were used to calculate the true stress and true strain values for martensite phase. Also, it may be noted that 05 pair of values (true stress and corresponding true strain) for each phase were determined in the present research (though larger number of values may provide even better results, but also increase the number of iterations). These 05 pair of values were selected randomly from the entire spectrum of engineering stress-strain values (of the tensile curve), with the care that values close to zero strain, to some intermediate values, till the maximum strain were covered. Thereafter, the true stress and true strain values were calculated using standard formula of true stress (Equation 1) and true strain (Equation 2).

$$\sigma_t = \sigma(1 + \varepsilon) \quad \ldots\ldots\ldots\ldots\ldots (1)$$

$$\varepsilon_t = ln(1 + \varepsilon) \quad \ldots\ldots\ldots\ldots\ldots (2)$$

where, σ_t is true stress (MPa), σ is engineering stress (MPa), ε is engineering strain, and ε_t is true strain.

Table 4.2 Property inputs for the constituent phases.

Plastic properties of the constituent phases of			
FERRITE		**MARTENSITE**	
True stress, σ_t (MPa)	**True Strain, ε_t**	**True stress, σ_t (MPa)**	**True Strain, ε_t**
175	0	600	0
405	0.01242	707	0.00995
459	0.01980	810.4	0.0129
609.5	0.05826	865.3	0.0178
649.8	0.079	922.5	0.02469
*** Young's modulus (E) and Poisson's ratio for the steel was taken as 2×10^5 GPa and 0.2 respectively.**			

Taking the above discussed inputs, simulation was conducted. In the present simulation work, the above mentioned 05 pair of stress-strain values were processed by the software in 23 increments, and the first significant visual output from the simulation effort was obtained after the 19th increment. Simulation results for the CAL processed microstructure (modelled DP-C steel containing MVF = 20%) with regards to distribution of stress (S, Mises stress) and equivalent plastic strain (PEEQ) is presented in Figure 4.9 and Figure 4.10 respectively.

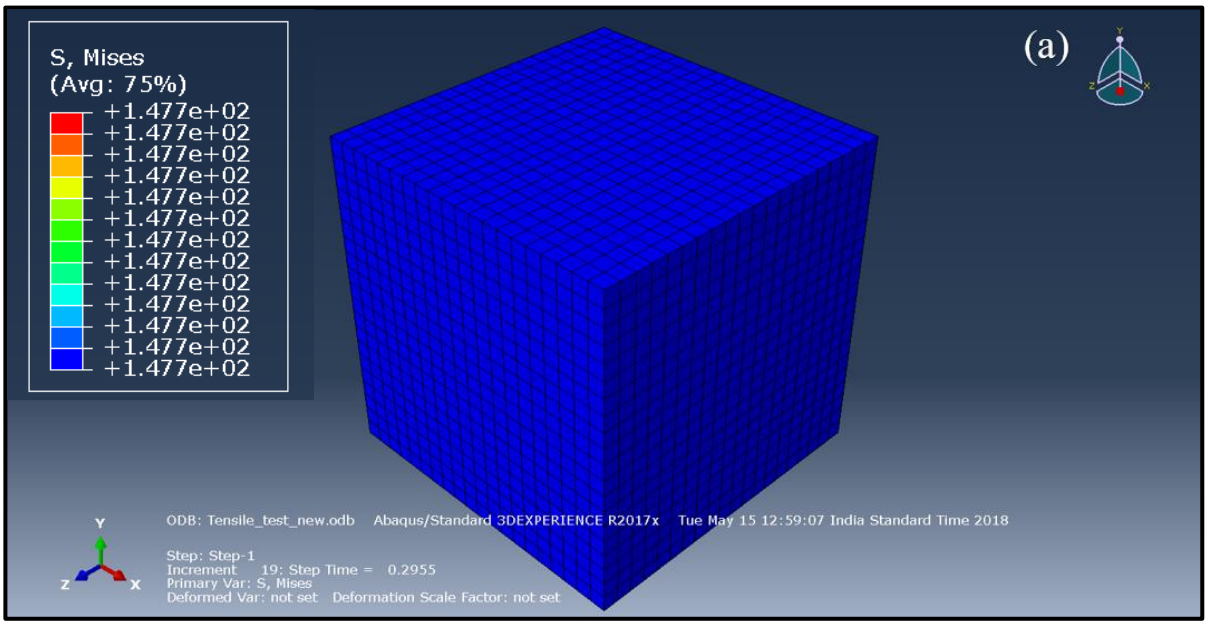

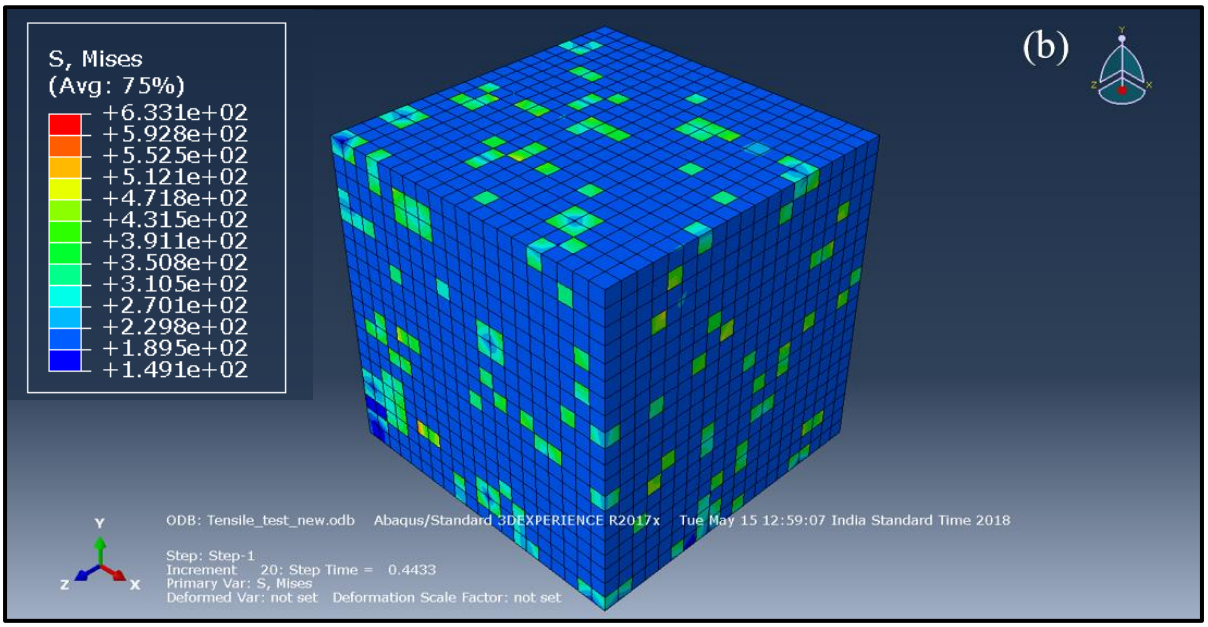
S, Mises
(Avg: 75%)
+6.331e+02
+5.928e+02
+5.525e+02
+5.121e+02
+4.718e+02
+4.315e+02
+3.911e+02
+3.508e+02
+3.105e+02
+2.701e+02
+2.298e+02
+1.895e+02
+1.491e+02
(b)
ODB: Tensile_test_new.odb Abaqus/Standard 3DEXPERIENCE R2017x Tue May 15 12:59:07 India Standard Time 2018
Step: Step-1
Increment 20: Step Time = 0.4433
Primary Var: S, Mises
Deformed Var: not set Deformation Scale Factor: not set

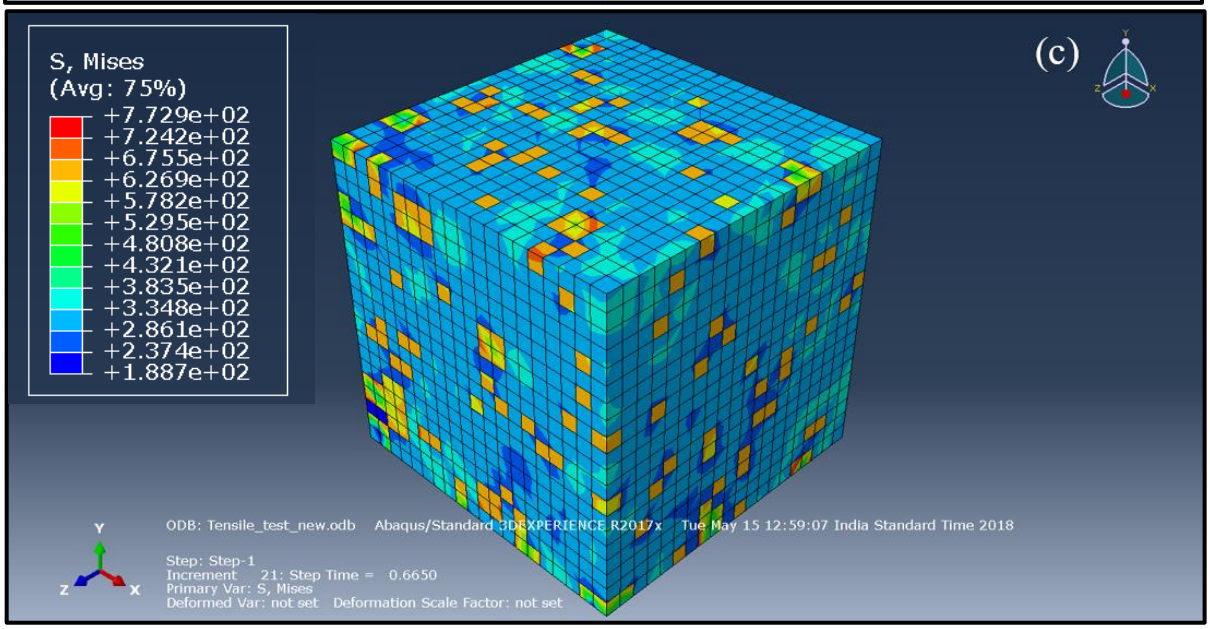
S, Mises
(Avg: 75%)
+7.729e+02
+7.242e+02
+6.755e+02
+6.269e+02
+5.782e+02
+5.295e+02
+4.808e+02
+4.321e+02
+3.835e+02
+3.348e+02
+2.861e+02
+2.374e+02
+1.887e+02
(c)
ODB: Tensile_test_new.odb Abaqus/Standard 3DEXPERIENCE R2017x Tue May 15 12:59:07 India Standard Time 2018
Step: Step-1
Increment 21: Step Time = 0.6650
Primary Var: S, Mises
Deformed Var: not set Deformation Scale Factor: not set

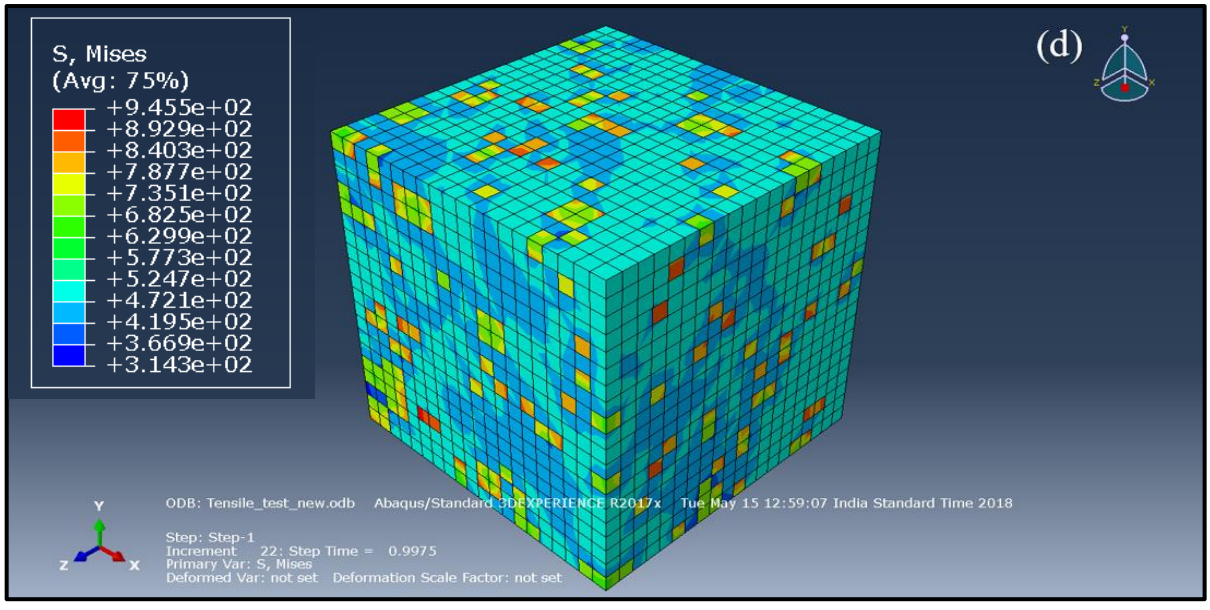
S, Mises
(Avg: 75%)
+9.455e+02
+8.929e+02
+8.403e+02
+7.877e+02
+7.351e+02
+6.825e+02
+6.299e+02
+5.773e+02
+5.247e+02
+4.721e+02
+4.195e+02
+3.669e+02
+3.143e+02
(d)
ODB: Tensile_test_new.odb Abaqus/Standard 3DEXPERIENCE R2017x Tue May 15 12:59:07 India Standard Time 2018
Step: Step-1
Increment 22: Step Time = 0.9975
Primary Var: S, Mises
Deformed Var: not set Deformation Scale Factor: not set

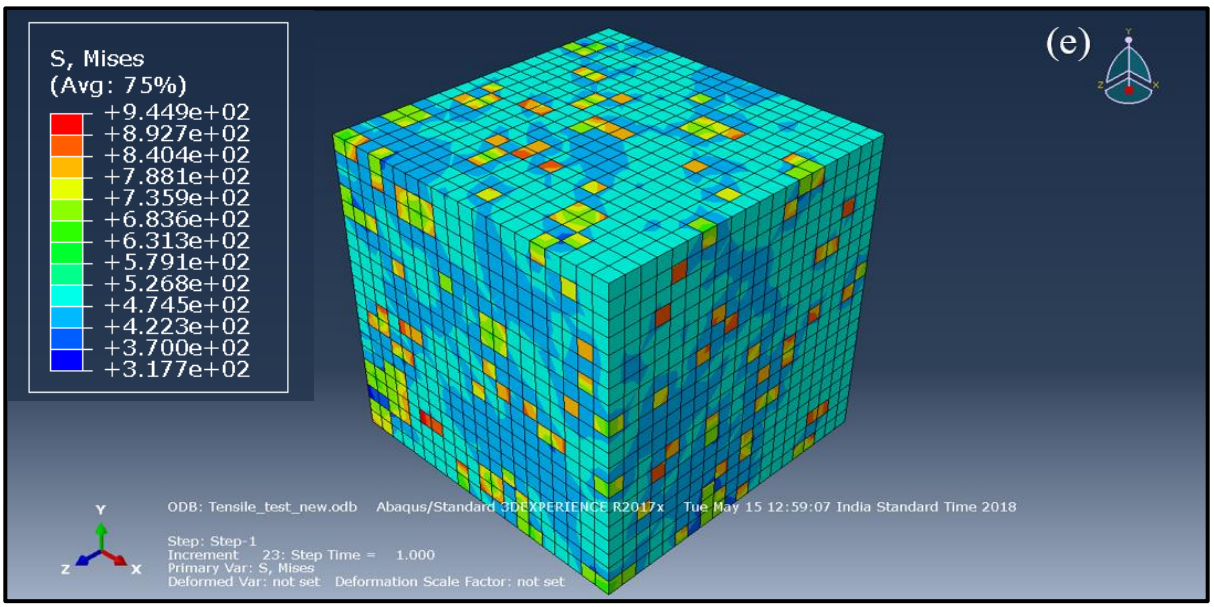

Figure 4.9 Stress concentration on the DP-C microstructure with MVF 20% (a–e) represents the significant increments from 19–23.

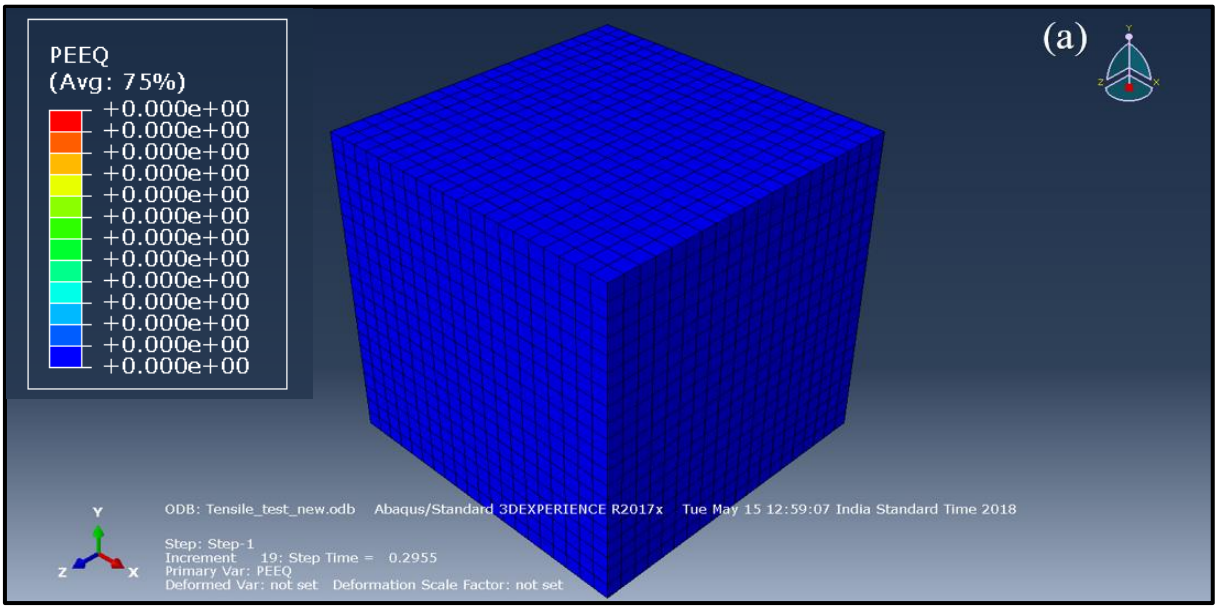

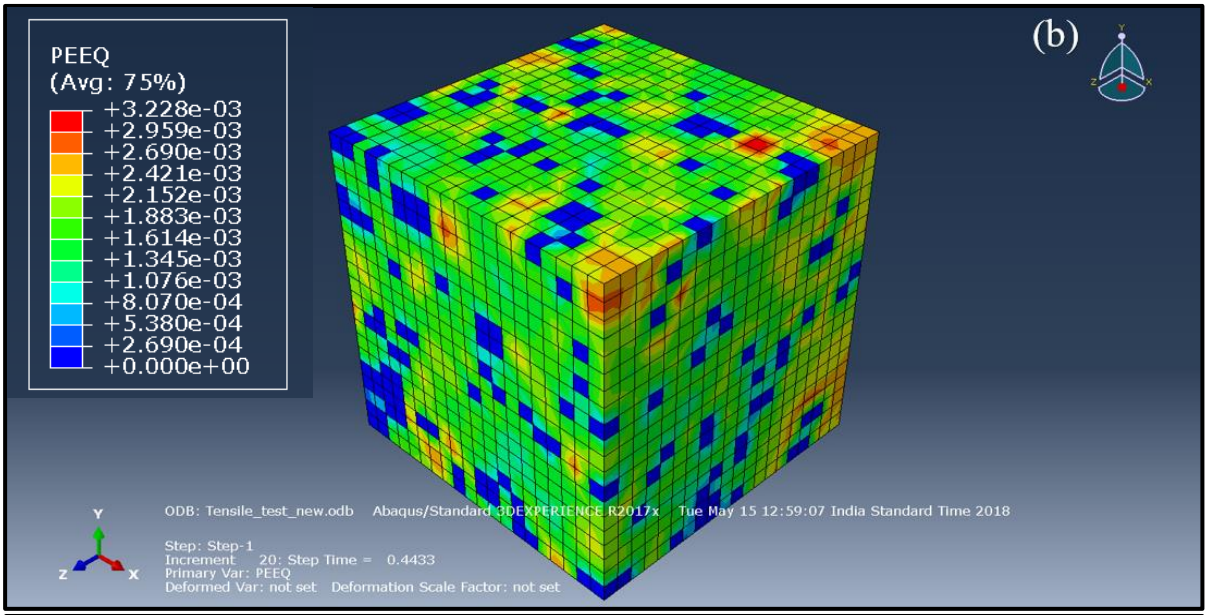
(b)
PEEQ
(Avg: 75%)
+3.228e-03
+2.959e-03
+2.690e-03
+2.421e-03
+2.152e-03
+1.883e-03
+1.614e-03
+1.345e-03
+1.076e-03
+8.070e-04
+5.380e-04
+2.690e-04
+0.000e+00
ODB: Tensile_test_new.odb Abaqus/Standard 3DEXPERIENCE R2017x Tue May 15 12:59:07 India Standard Time 2018
Step: Step-1
Increment 20: Step Time = 0.4433
Primary Var: PEEQ
Deformed Var: not set Deformation Scale Factor: not set

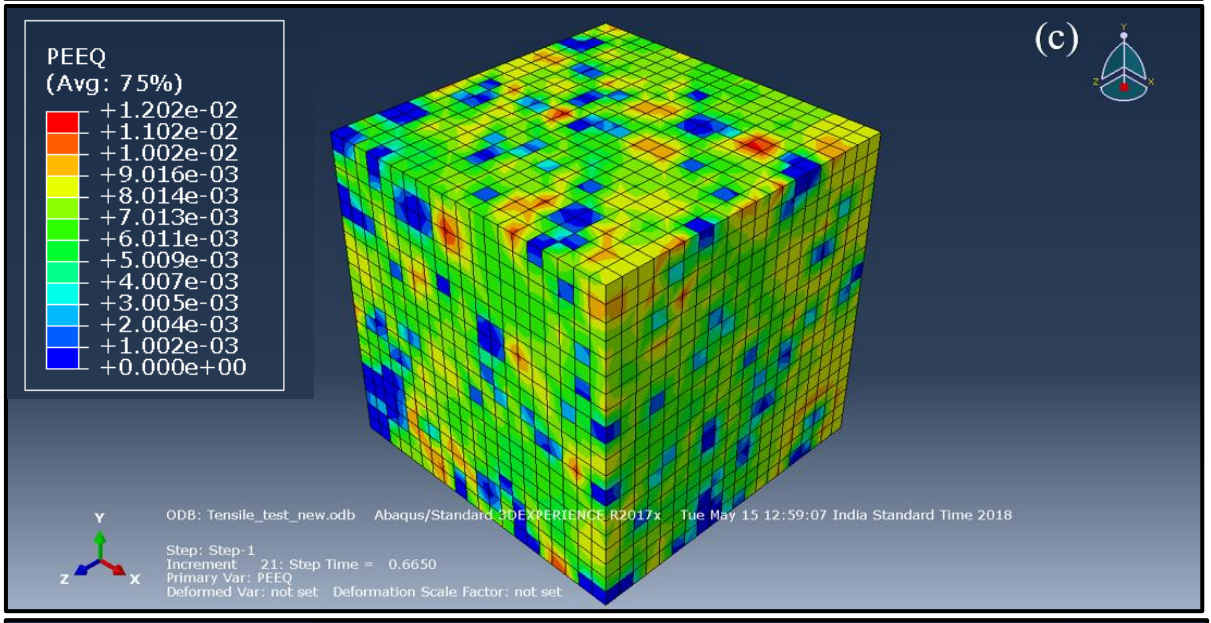
(c)
PEEQ
(Avg: 75%)
+1.202e-02
+1.102e-02
+1.002e-02
+9.016e-03
+8.014e-03
+7.013e-03
+6.011e-03
+5.009e-03
+4.007e-03
+3.005e-03
+2.004e-03
+1.002e-03
+0.000e+00
ODB: Tensile_test_new.odb Abaqus/Standard 3DEXPERIENCE R2017x Tue May 15 12:59:07 India Standard Time 2018
Step: Step-1
Increment 21: Step Time = 0.6650
Primary Var: PEEQ
Deformed Var: not set Deformation Scale Factor: not set

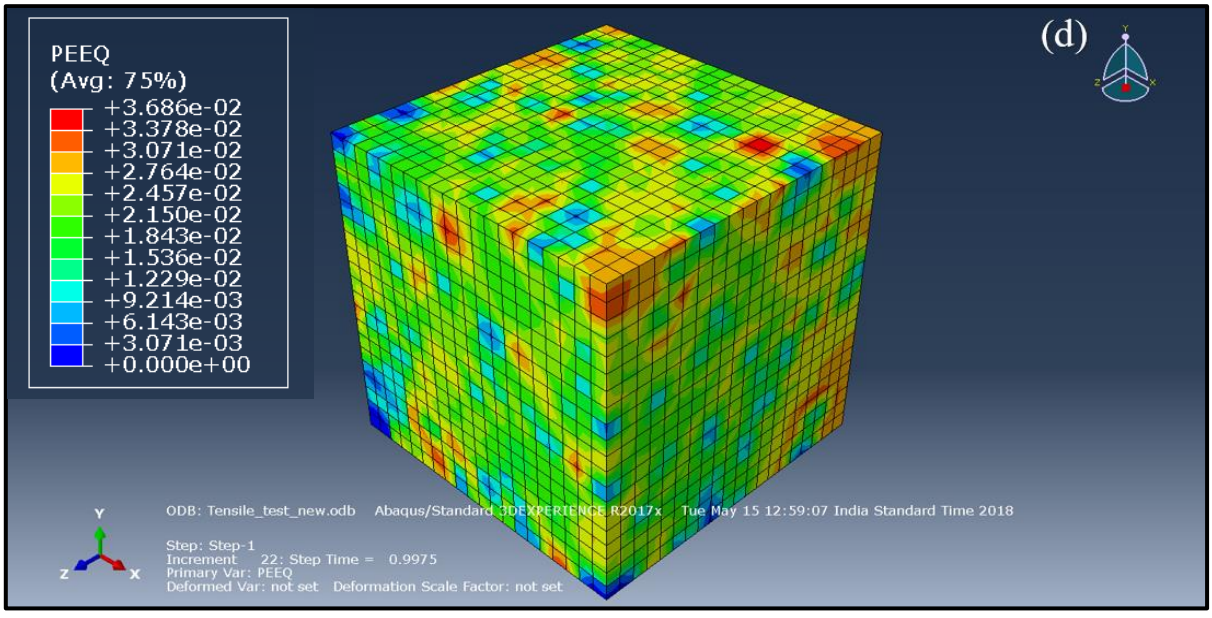
(d)
PEEQ
(Avg: 75%)
+3.686e-02
+3.378e-02
+3.071e-02
+2.764e-02
+2.457e-02
+2.150e-02
+1.843e-02
+1.536e-02
+1.229e-02
+9.214e-03
+6.143e-03
+3.071e-03
+0.000e+00
ODB: Tensile_test_new.odb Abaqus/Standard 3DEXPERIENCE R2017x Tue May 15 12:59:07 India Standard Time 2018
Step: Step-1
Increment 22: Step Time = 0.9975
Primary Var: PEEQ
Deformed Var: not set Deformation Scale Factor: not set

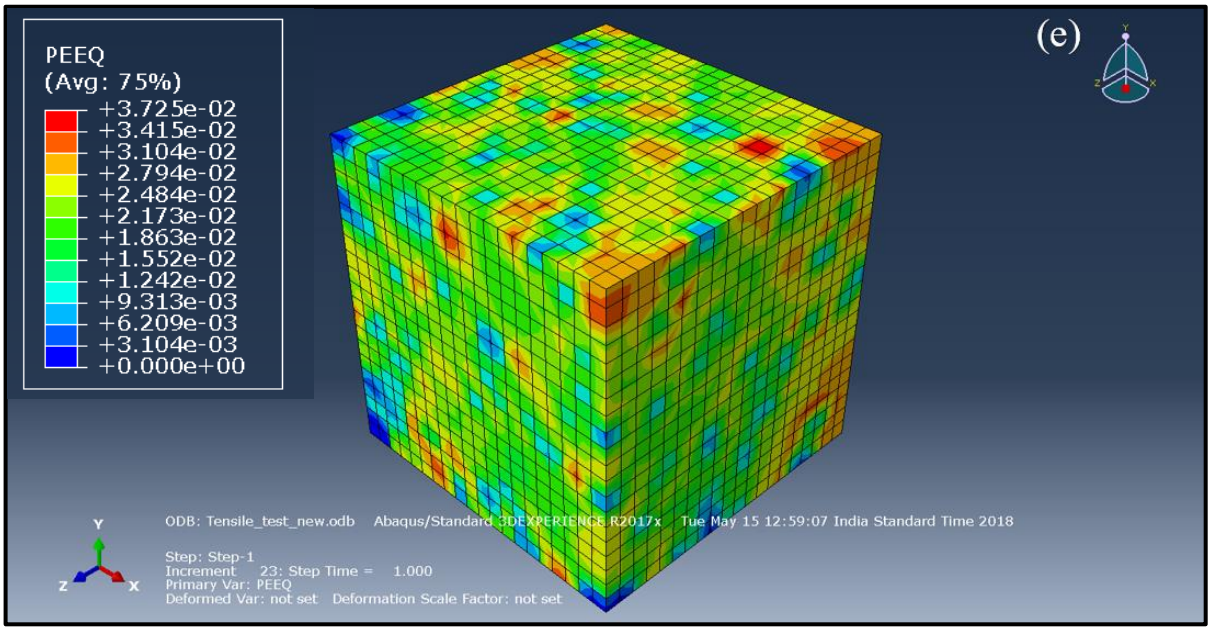

Figure 4.10 Equivalent plastic strain on the DP-C microstructure with MVF 20% (a–e) represents the significant increments from 19–23.

To understand the tensile deformation behavior of CAL processed steel, Figure 4.8a, Figure 4.9e, Figure 4.10e, and Figure 4.11 are considered.

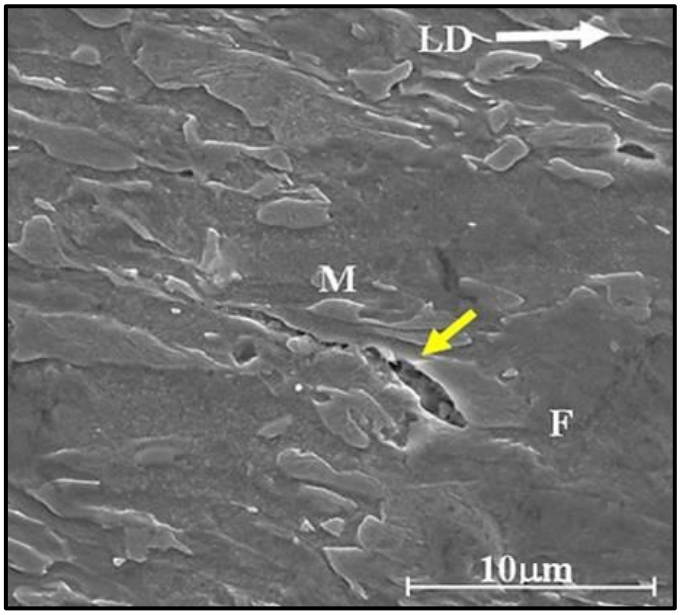

Figure 4.11 SEM micrograph of the DP steel processed through CAL process. M = martensite, F = ferrite [33].

For the CAL processed DP steel in the present research (DP-C steel; MVF: 22%), the UTS and TE values were 631 MPa and 28% respectively. Singh *et al.* (2017) obtained DP microstructure (MVF: 19%; UTS: 586 MPa, TE: 26.8%) in a similar steel after CAL processing. The authors discussed the fracture behaviour of the tensile tested DP steel (see Figure 4.11) and the same

is being considered as representative microstructure/fracture behaviour of the DP-C steel processed in the present work. It was reported that the damage mechanism mostly originated at the ferrite-martensite interface regions, propagated further, and created a total damage. The authors stated that martensite phase present in the microstructure resisted deformation while ferrite phase acted totally opposite, resulting in micro-cracking and voids initiation/propagation at the ferrite-martensite interface regions of the microstructure. High ductility of the CAL processed steel was attributed to the combined effect of martensite resistance and smooth strain behaviour of ferrite. Moreover, the authors reported that ductility was high as it (DP-C) was a ferrite-based steel, with ferrite fraction as 81% [33].

The simulation results for the CAL processed DP-C steel compare well with the experimental ones, with regards to deformation behaviour/damage mechanisms shown by the steel. Dream.3D generated the said microstructure (with MVF = 20%) as shown in Figure 4.8a. Abaqus simulated the stress (Figure 4.9e) and strain (Figure 4.10e) distribution in the DP-C microstructure. Experimental results (reported literature; Singh *et al.* 2017) showed that micro-cracking at ferrite-martensite interfaces was the main deformation mechanism. For the simulation results showing stress distribution (Figure 4.9e), it was observed that stress was mainly generated in regions of microstructure containing martensite. For the other regions mainly constituted by ferrite phase, stress varied from low to moderate values (see Figure 4.8a and Figure 4.9e). The overall effect was a moderate ultimate stress value of 631 MPa for the DP-C steel. Further, for the simulation results showing strain distribution (Figure 4.10e), it was observed that less (or minimal) plastic strain values were shown for regions of microstructure containing martensite phase (see Figure 4.8a and Figure 4.10e). Similarly, regions containing ferrite phase in the vicinity of martensite regions also showed low values of plastic strain. However, as expected, maximum plastic strain was accommodated by regions containing ferrite phase (away from martensite regions). Since, bulk of the microstructure comprised of the soft/ductile ferrite phase which showed extensive plastic strain (in the simulation results), the given DP-C steel could display good value of percentage elongation (as also shown under tensile test; TE = 28%). Further, with regards to damage mechanism, the simulation results also indicated that micro-cracks/voids would initiate at the ferrite-martensite interface because of the very diverse nature of constituent phases in accommodating plastic strain (ferrite accommodates large plastic strain whereas martensite shows least accommodation).

To understand the tensile deformation behaviour of CAS-4 processed steel (i.e. HM-4 steel), Figure 4.7h, 4.8b, 4.12e, and 4.13e are considered. The experimental results pertaining to tensile testing and subsequent characterization (fractographic analysis) of HM-4 steel were

discussed in Section 4.3 and Section 4.4 respectively. For HM-4 steel (MVF: 62.2%), the UTS and TE values obtained were 1052 MPa and 12% respectively. It was discussed (Section 4.4) that HM-4 steel (Figure 4.7g–h) consisting of more prominent core/shell type harmonic microstructure and displayed very limited martensite micro-cracking tendency. Both, core (primary martensite region) as well as shell (ferrite region) of the DP microstructure showed extensive plastic deformation or plastic strain compatibility. Therefore, even with large fraction of martensite in these microstructures (DP-3/DP-4), the onset of damage activity at ferrite-martensite interface was delayed and that at martensite inter-lath was avoided. Further, damage activity was observed to be mostly restricted at shell/core interfaces (ferrite-martensite interfaces).

The simulation results compared well with experimental ones w.r.t deformation behaviour/damage mechanisms shown by HM-4 steel. HM-4 microstructure (MVF: 62%) was generated by Dream.3D (Figure 4.8b) and stress-strain behaviour was simulated in Abaqus (Figure 4.12e and Figure 4.13e).

For the simulation results showing stress distribution, it was observed that stress was mainly generated in regions of microstructure containing martensite phase (see Figure 4.8b and Figure 4.12e).

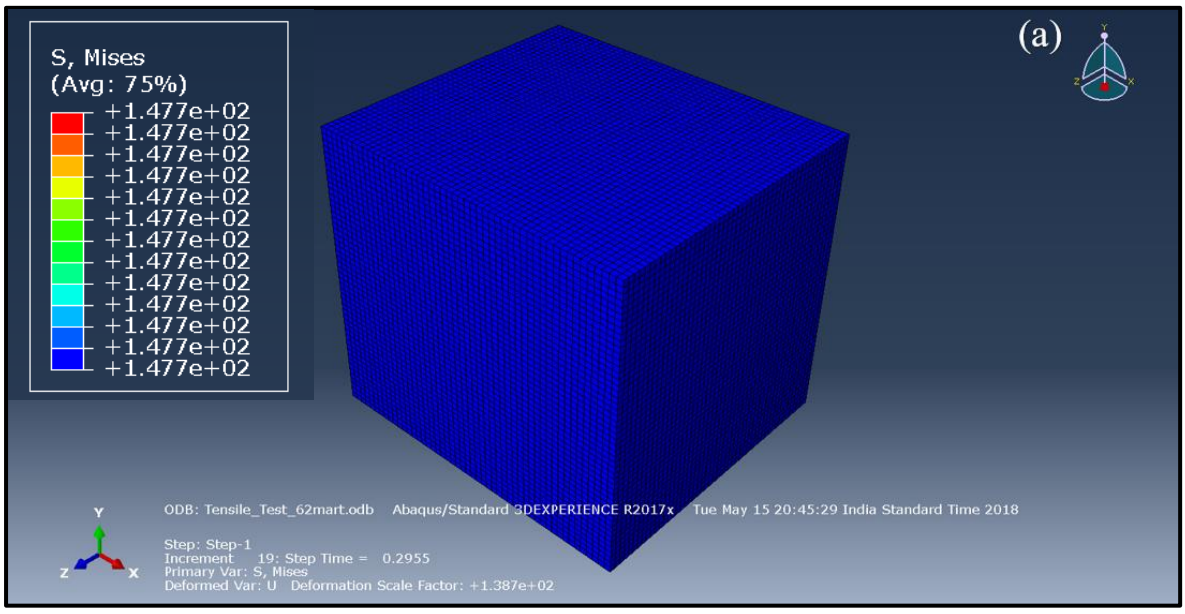

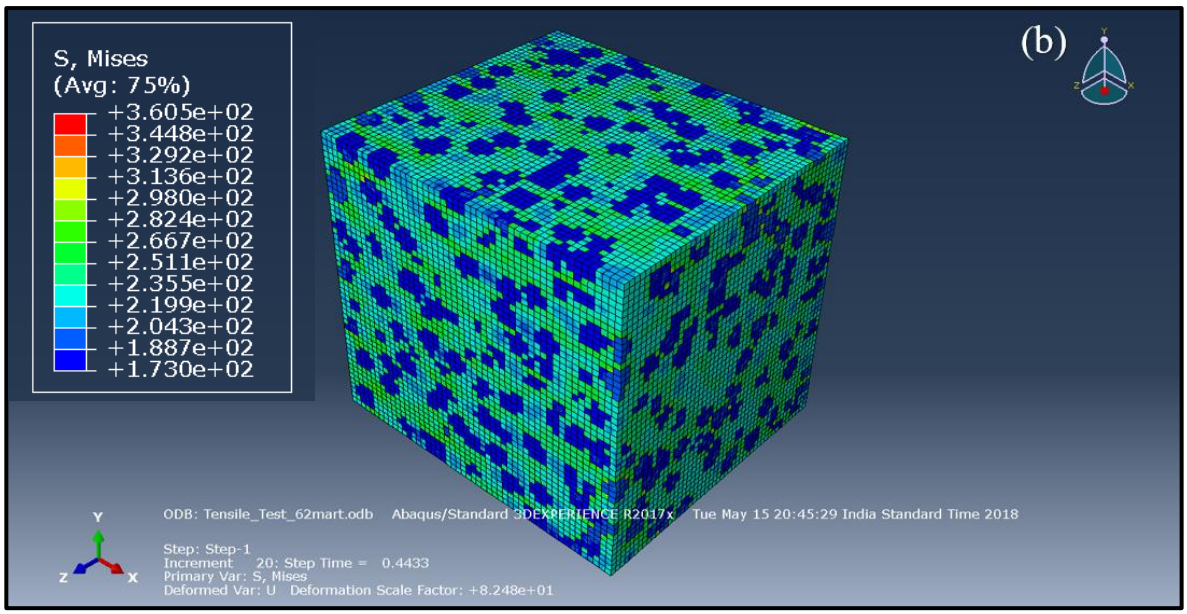
S, Mises
(Avg: 75%)
+3.605e+02
+3.448e+02
+3.292e+02
+3.136e+02
+2.980e+02
+2.824e+02
+2.667e+02
+2.511e+02
+2.355e+02
+2.199e+02
+2.043e+02
+1.887e+02
+1.730e+02
(b)
ODB: Tensile_Test_62mart.odb Abaqus/Standard 3DEXPERIENCE R2017x Tue May 15 20:45:29 India Standard Time 2018
Step: Step-1
Increment 20: Step Time = 0.4433
Primary Var: S, Mises
Deformed Var: U Deformation Scale Factor: +8.248e+01

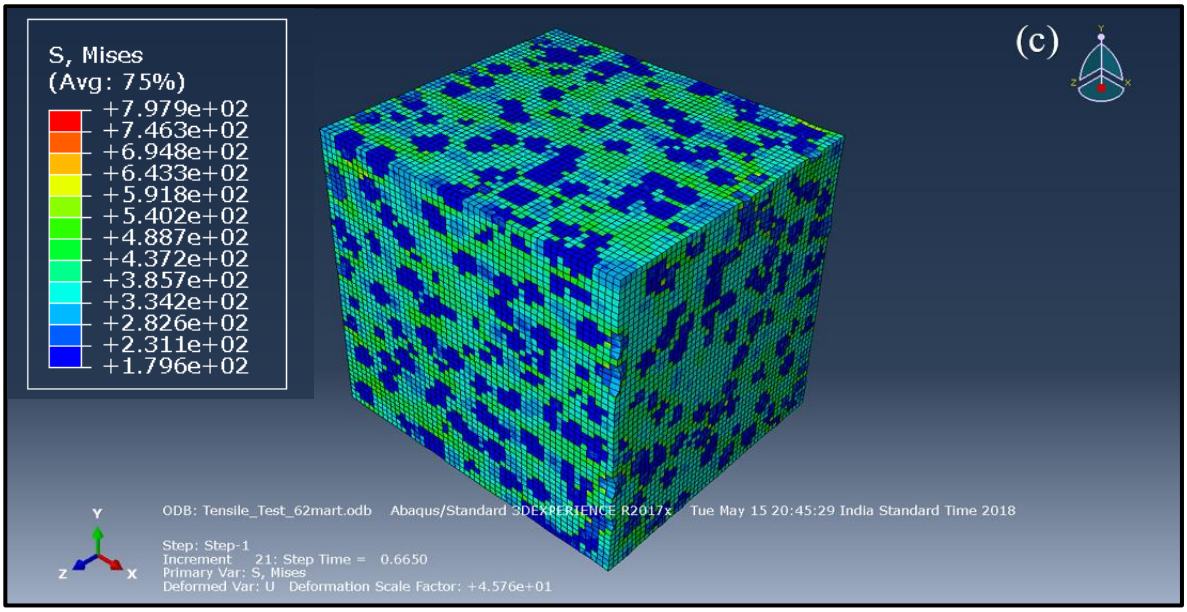
S, Mises
(Avg: 75%)
+7.979e+02
+7.463e+02
+6.948e+02
+6.433e+02
+5.918e+02
+5.402e+02
+4.887e+02
+4.372e+02
+3.857e+02
+3.342e+02
+2.826e+02
+2.311e+02
+1.796e+02
(c)
ODB: Tensile_Test_62mart.odb Abaqus/Standard 3DEXPERIENCE R2017x Tue May 15 20:45:29 India Standard Time 2018
Step: Step-1
Increment 21: Step Time = 0.6650
Primary Var: S, Mises
Deformed Var: U Deformation Scale Factor: +4.576e+01

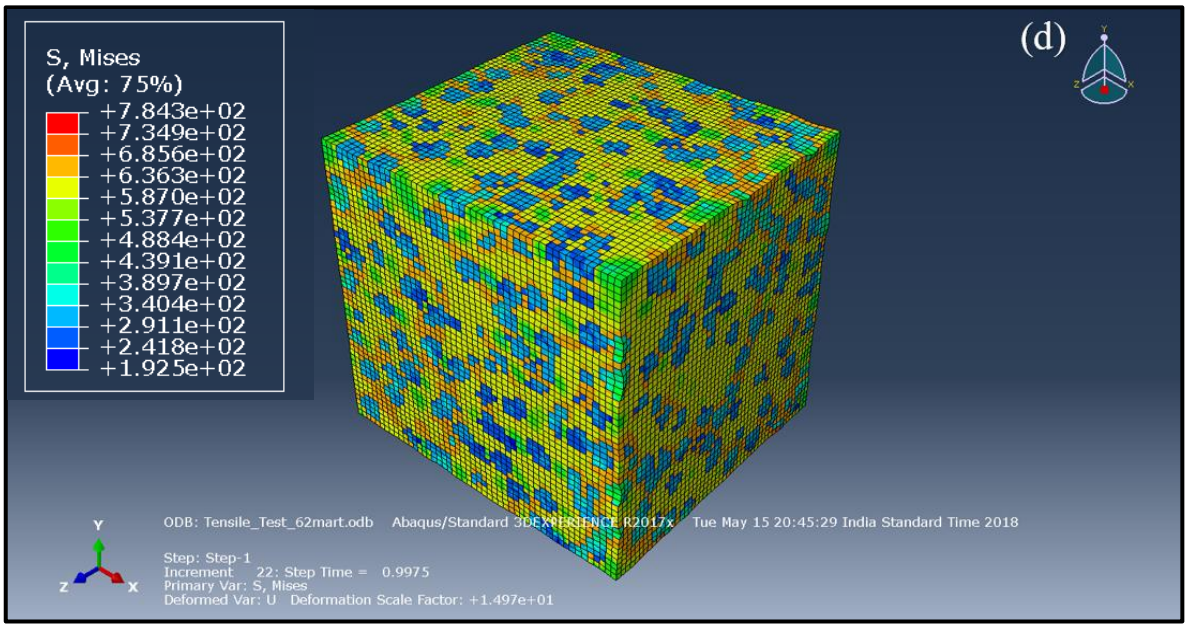
S, Mises
(Avg: 75%)
+7.843e+02
+7.349e+02
+6.856e+02
+6.363e+02
+5.870e+02
+5.377e+02
+4.884e+02
+4.391e+02
+3.897e+02
+3.404e+02
+2.911e+02
+2.418e+02
+1.925e+02
(d)
ODB: Tensile_Test_62mart.odb Abaqus/Standard 3DEXPERIENCE R2017x Tue May 15 20:45:29 India Standard Time 2018
Step: Step-1
Increment 22: Step Time = 0.9975
Primary Var: S, Mises
Deformed Var: U Deformation Scale Factor: +1.497e+01

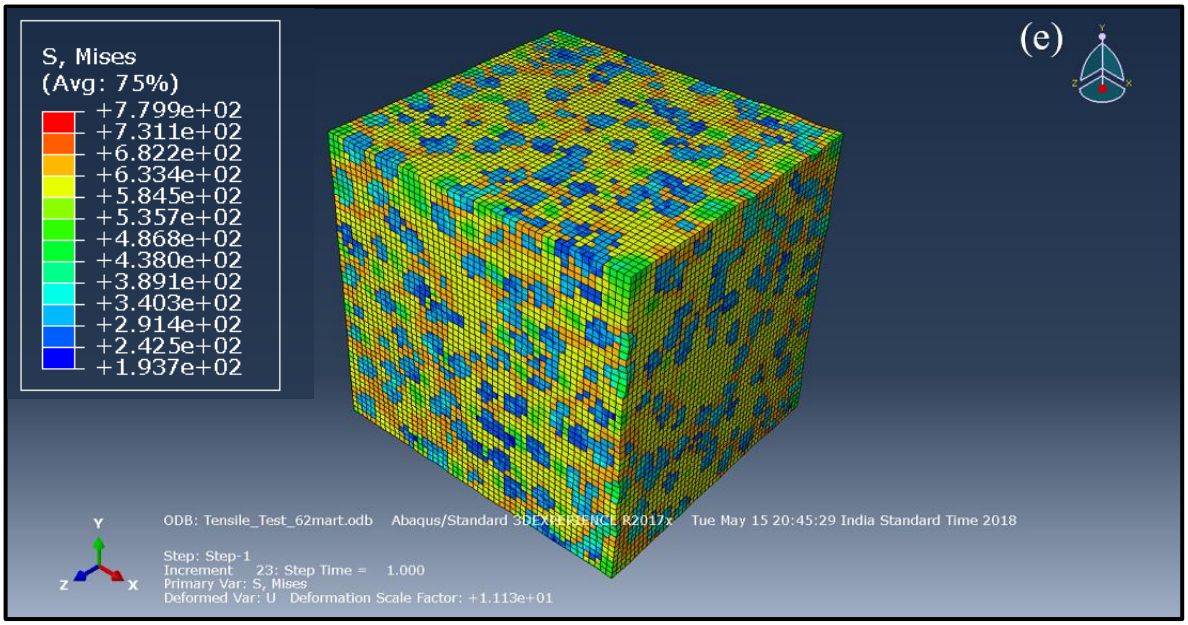

Figure 4.12 Stress concentration on the HM-4 microstructure with MVF 62% (a–e) represent the significant increments from 19–23.

Martensite regions showed high stress accommodation. Interestingly, martensite regions adjoining to ferrite regions showed even higher values of stress. Further, martensite was the primary phase comprising the HM-4 microstructure (MVF = 62%). This all resulted in very high value of UTS for the HM-4 steel as compared to DP-C steel (1054 MPa in comparison to 631 MPa for DP-C steel; compare stress distribution in Figure 4.12e and Figure 4.9e).

Further, for the simulation results showing strain distribution (Figure 4.13e), it was observed that less (or minimal) plastic strain values were shown for regions of microstructure containing martensite phase (see Figure 4.8b and Figure 4.13e).

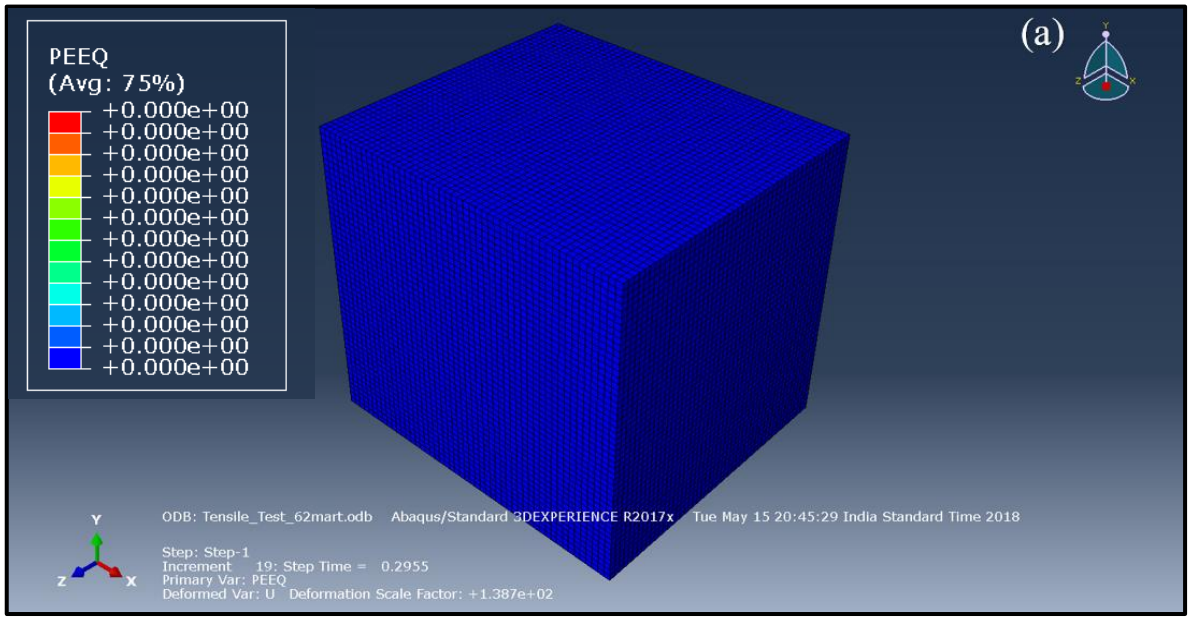

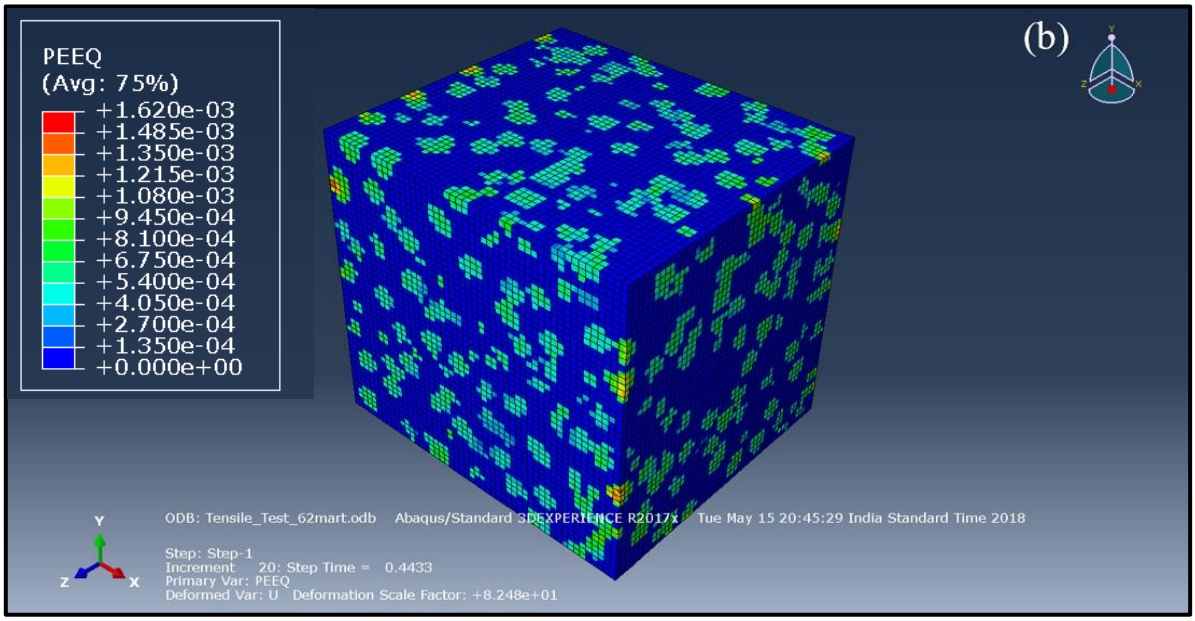
PEEQ
(Avg: 75%)
+1.620e-03
+1.485e-03
+1.350e-03
+1.215e-03
+1.080e-03
+9.450e-04
+8.100e-04
+6.750e-04
+5.400e-04
+4.050e-04
+2.700e-04
+1.350e-04
+0.000e+00
(b)
ODB: Tensile_Test_62mart.odb Abaqus/Standard 3DEXPERIENCE R2017x Tue May 15 20:45:29 India Standard Time 2018
Step: Step-1
Increment 20: Step Time = 0.4433
Primary Var: PEEQ
Deformed Var: U Deformation Scale Factor: +8.248e+01

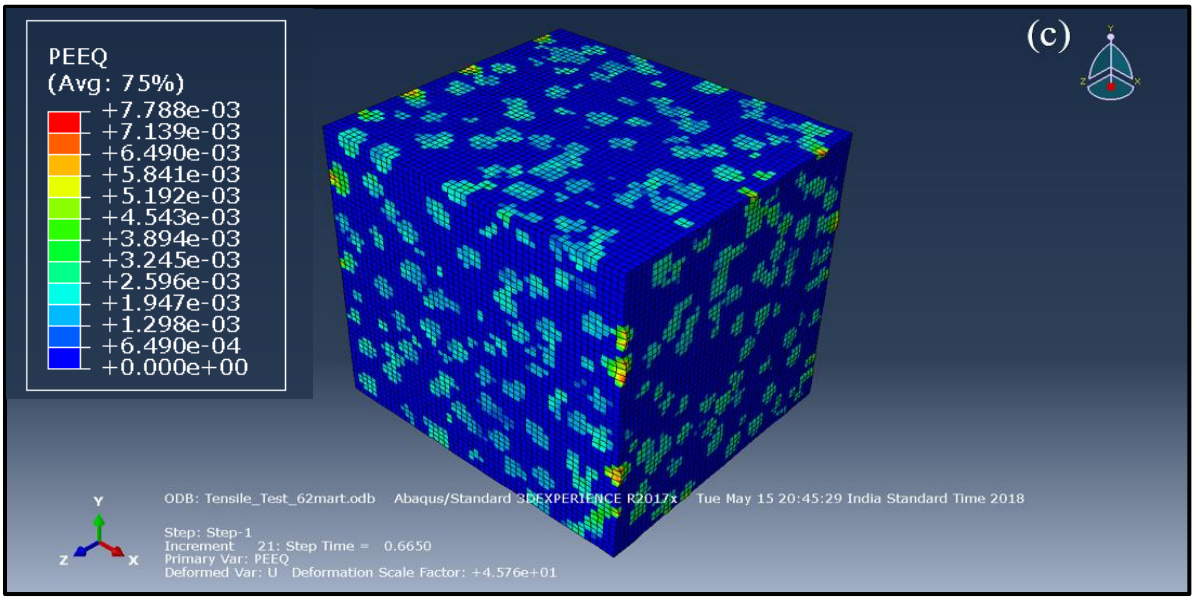
PEEQ
(Avg: 75%)
+7.788e-03
+7.139e-03
+6.490e-03
+5.841e-03
+5.192e-03
+4.543e-03
+3.894e-03
+3.245e-03
+2.596e-03
+1.947e-03
+1.298e-03
+6.490e-04
+0.000e+00
(c)
ODB: Tensile_Test_62mart.odb Abaqus/Standard 3DEXPERIENCE R2017x Tue May 15 20:45:29 India Standard Time 2018
Step: Step-1
Increment 21: Step Time = 0.6650
Primary Var: PEEQ
Deformed Var: U Deformation Scale Factor: +4.576e+01

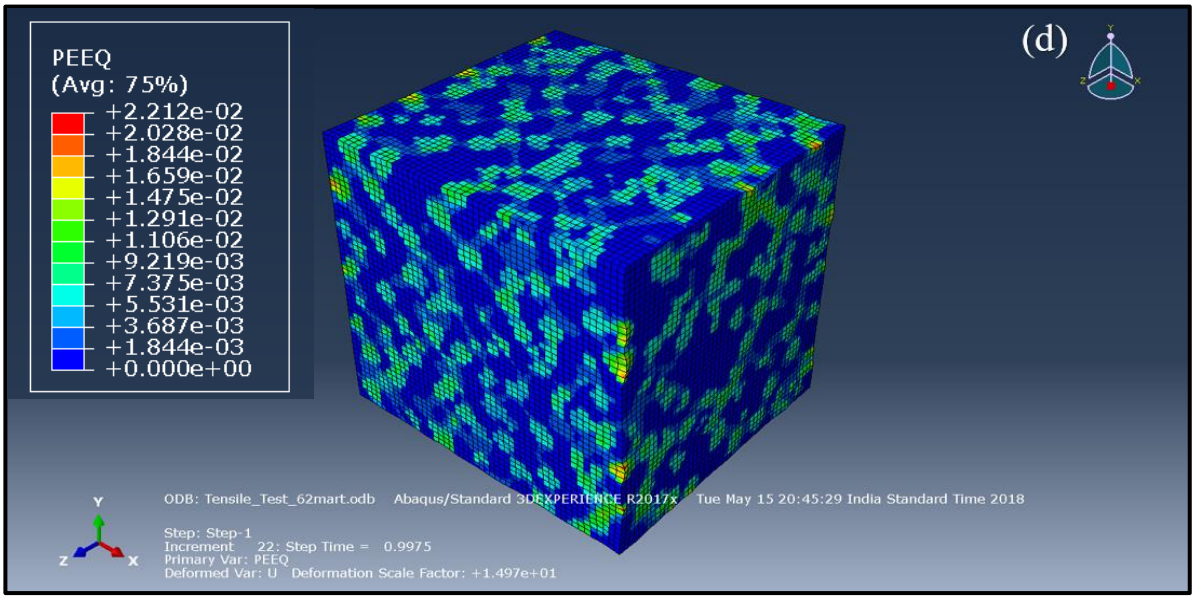
PEEQ
(Avg: 75%)
+2.212e-02
+2.028e-02
+1.844e-02
+1.659e-02
+1.475e-02
+1.291e-02
+1.106e-02
+9.219e-03
+7.375e-03
+5.531e-03
+3.687e-03
+1.844e-03
+0.000e+00
(d)
ODB: Tensile_Test_62mart.odb Abaqus/Standard 3DEXPERIENCE R2017x Tue May 15 20:45:29 India Standard Time 2018
Step: Step-1
Increment 22: Step Time = 0.9975
Primary Var: PEEQ
Deformed Var: U Deformation Scale Factor: +1.497e+01

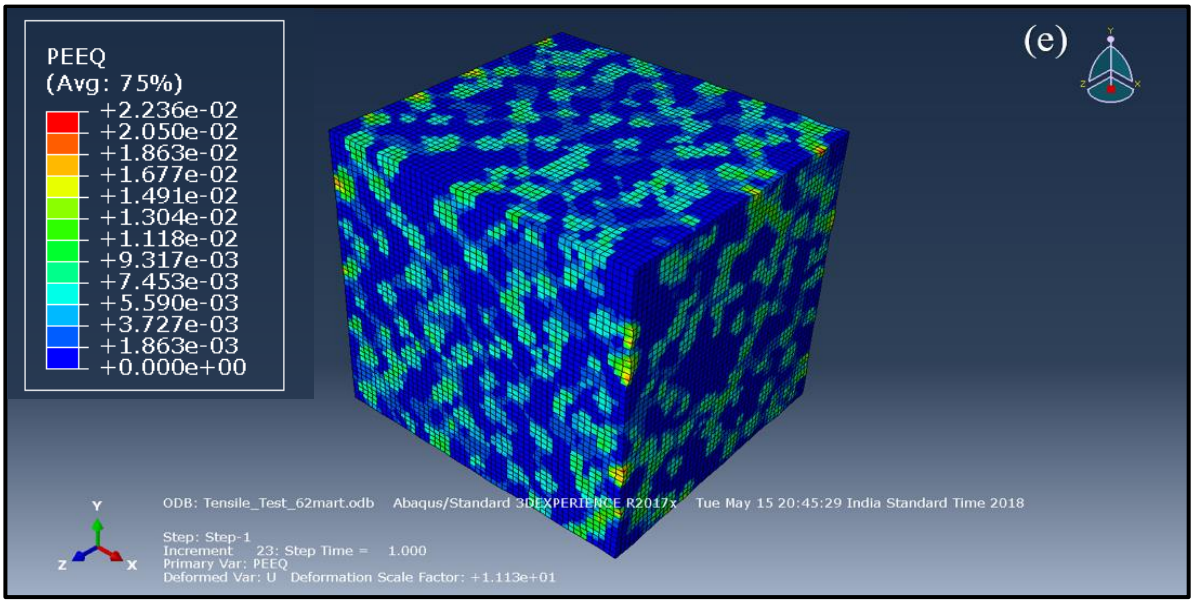

Figure 4.13 Equivalent plastic strain on the HM-4 microstructure with MVF 62% (a–e) represents the significant increments from 19–23.

Plastic strain was mainly accommodated by regions containing ferrite phase. Since, the HM-4 microstructure mainly comprised of martensite phase (which did not show significant plastic strain in the simulation results), the given HM-4 steel could display only a moderately low value of percentage elongation (also shown under tensile test; TE = 12%) as compared to DP-C steel. Interestingly, martensite and ferrite regions of microstructure did not show significantly very different plastic strain accommodation. Thus, it can be concluded that martensite-ferrite combination in HM-4 steels showed better strain compatibility as compared to DP-C steel. This observation from the simulation results compares well with experimental findings of fractographic analysis where microstructure of HM-4 steel showed significant plastic deformation of both ferrite and martensite phases.

Finally, with regards to damage mechanism, the simulation results also indicated that micro-cracks/voids would initiate at the core-shell interface regions (ferrite-martensite interfaces) because of the very diverse nature of constituent phases in accommodating stress. The stress distribution in ferrite was low whereas very high in martensite. Consequently, there was high stress incompatibility at ferrite-martensite interfaces resulting in micro-cracking/voids initiation at the core-shell interface regions. Thus, the main damage mechanism is again observed at ferrite-martensite interfaces.

CHAPTER 5
CONCLUSIONS

5.1 General

The present work was an attempt to develop various harmonic structured DP steels by changing the annealing process parameters and to observe their mechanical properties and fracture behaviour. Modelling of results pertaining to deformation behaviour was also performed. The main conclusions drawn from the present work are as follows:

5.2 Annealing simulations

- The steel processed by CAL route consisted of finely dispersed martensite islands in the ferrite matrix. Martensite islands were mainly present at the ferrite grain boundaries. For the CAS processed steels, HM-1 microstructure contained well distributed martensite packets of varied size ranges surrounded by ferrite phase network. In HM-2 microstructure, spacing between two cores was less, indicating refinement in the arrangement of core-shell structure repeatability. In HM-3, more distinct evolution of harmonic structure of core and shell type morphology was obtained and there was a transition from predominant ferrite based dual phase steel to martensite based dual phase steel. In HM-4, the core distribution was very fine as compared to other HM microstructures.
- Image J software was used for quantitative analysis of microstructures of DP steels (obtained by CAL and CAS cycles). MVF for DP steels obtained by CAL, CAS-1, CAS-2, CAS-3, and CAS-4 processes were 22%, 35.5%, 43.5%, 52.3%, and 62.2% respectively.

5.3 Tensile deformation

- Tensile strength of different microstructures viz. HM-1–HM-4 increased with increase in MVF. A significant change in tensile properties was seen between HM-2 and HM-3 microstructures, although, MVF change was only about 9%. The tensile strength of HM-4 (MVF=62.2 %) was higher in comparison to HM-3 (MVF=52.3 %) microstructure without any loss in ductility. This was attributed to refinement of harmonic structure.

5.4 Microstructure characterization of deformed samples

- In DP-C microstructure, the crack originated at ferrite-martensite interface, which propagates further and caused total damage.
- In HM-1 and HM-2 microstructures, the cracks mostly originated at fine martensite laths and ferrite-martensite interface.
- In HM-3 and HM-4 microstructures, there was very limited micro-cracking of martensite in the tensile necking zone. However, ferrite-martensite interface and martensite inter-lath damage activity was restricted and both ferrite and martensite revealed plastic strain compatibility. Thus, it was concluded that by controlling the martensite morphology and MVF, the deformation mechanism of DP steel can be controlled.

5.5 Modelling and simulation

- Microstructures obtained by CAL and CAS-4 (i.e. DP-C and HM-4 respectively) were successfully modelled using Dream.3D software. Further, simulation results using Abaqus software were able to appropriately predict the deformation behaviour of DP steels. Good agreement between predicted simulation results and experimental results was observed with regards to deformation behaviour shown by different DP steels.
- Simulation results for DP-C microstructure (MVF = 22%) showed that during tensile deformation, stress was mainly generated in regions of microstructure containing martensite phase. For regions containing ferrite phase, stress varied from low to moderate values only. Further, maximum plastic strain was accommodated by regions containing ferrite phase (away from martensite regions). Plastic strain values for regions containing martensite was minimal. Because of this diverse nature of constituent phases in accommodating plastic strain, micro-cracks/voids were initiated at the ferrite-martensite interface.

  Simulation results for HM-4 microstructure (MVF = 62%) depicted that stress was mainly generated in regions of microstructure containing martensite phase. Martensite regions showed high stress accommodation. Interestingly, martensite regions adjoining to ferrite regions showed even higher values of stress. Plastic strain was mainly accommodated by regions containing ferrite phase. However, martensite and ferrite regions of microstructure did not show significantly very different plastic strain accommodation. Martensite-ferrite combination in HM-4 steels provides a better strain compatibility as compared to DP-C steel. Again, micro-cracks/voids initiated at the ferrite-martensite interface. This was a result of high stress incompatibility at ferrite-martensite interfaces resulting in micro-

cracking/voids initiation at the core-shell interface regions. Thus, the main damage mechanism was again observed at ferrite-martensite interfaces.

5.6 Major conclusions

There is an increasing demand of steels possessing high strength and good ductility. In the present dissertation work, changes brought in martensite fraction and martensite morphology played a key role in developing DP steels with high strength-ductility combination.

The main conclusions are as follows:

- Steels processed by CAS annealing route produce DP steels with core-shell microstructure (called harmonic structure) and display higher yield strength and ultimate tensile strength with slightly reduced percentage elongation as compared to DP steels processed by the industrially used CAL annealing route. This shows that tensile properties of DP steels can be significantly changed by altering martensite fraction and distribution.
- Attempts to model DP microstructures and also to simulate their tensile deformation behaviour were successful. Modelled microstructures when simulated were able to depict the deformation behaviour of ferrite and martensite phases under loading conditions (similar to the experimental results obtained by tensile testing of DP steels).
- For steels to possess excellent strength-ductility combination, the volume fraction, morphology, and distribution of phases of DP steels should be such that the constituent phases should have good stress compatibility as well as good strain compatibility between ferrite and martensite phases. If either strain incompatibility or stress incompatibility between the constituent phases is poor, micro-cracks/voids initiation begin at ferrite-martensite interface.

5.7 Scope for future work

The following presents the scope for future work.

- For the DP steels processed in the present work, testing was conducted to determine the tensile properties (yield strength, ultimate tensile strength, and percentage elongation) of steels possessing different DP microstructures. Subsequent to testing, characterization of fracture surfaces of tensile specimens of various microstructures was done to determine the reasons for properties displayed and the damage/failure mechanisms present. However, this entire analysis was for quasi-static strain rate conditions. The present work can be extended

to correlate the microstructure and tensile properties when testing is done under high strain conditions which are significant for crash conditions.

- In the present work, the DP microstructures investigated comprised of ferrite and martensite phases. For both type of DP microstructures viz. conventional DP-C steel (i.e. CAL processed) and the CAS processed (HM-1–HM-4 steels), either strain incompatibility or stress incompatibility between constituent phases of ferrite and martensite was noted. The present experimental and simulation work can be extended for DP steels containing ferrite and bainite as the constituent phases.

REFERENCES

1. A. Uenishi, H. Yoshida, S. Yonemura, S. Hiwatashi, S. Hirose, and N. Suzuki, High strain rate properties of high strength steel sheets, *International Journal of Automobile Engineering*, 2, 109–113, 2011.
2. E. Cadoni, N.K. Singh, M.K. Singh, and N.K. Gupta, Strain rate behaviour of multi-phase and complex-phase steels for automotive applications, *EPJ Web of Conferences*, 26 (05003), 1–6, 2012.
3. J. Slycken, P. Verleysen, J. Degrieck, and J. Bouquerel, Characterisation of the high strain rate properties of advanced high strength steels, *High Performance Structures and Materials III*, 85, 259–268, 2006.
4. M. Isakova, M. May, S. Hiermaier, and V.T. Kuokkala, A model for the strain rate dependent plasticity of a metastable austenitic stainless steel, *Materials and Design*, 106, 258–272, 2016.
5. A. Uenishi, H. Yoshida, Y. Kuriyama, and M. Takahashi, Material characterization at high strain rates for optimizing car body structures for crash events, *Nippon Steel Technical Report No.* 88, 22–26, 2003.
6. S. Keeler and M. Kimkchi, Advanced high strength steels applications guidelines version 5.0, *World Auto Steel*, 2014.
7. R. Kuziak, R. Kawalla, and S. Waengler, Advanced high strength steels for automotive industry, *Archives of Civil and Mechanical Engineering*, 8, 103–117, 2008.
8. M. Mukherjee, T. Bhattacharyya, and S.B. Singh, Models for austenite to martensite transformation in TRIP-aided steels: a comparative study, *Materials and Manufacturing Processes*, 25(1–3), 206–210, 2010.
9. P. Simon and P.D. Beggs, A numerical performance comparison of a dual-phase steel and aluminium alloy bumper bar system, *International Journal of Crashworthiness*, 15, 425–442, 2010.
10. Q.U. Hao, Advanced high strength steel through para equilibrium carbon partitioning and austenite stabilization, Ph.D. Thesis, Case Western Reserve University, USA, 2011.
11. O.N. Cora and M. Koc, Promises and problems of ultra/advanced high strength steel (U/AHSS) utilization in automotive industry, In: *Proceedings of the 7th Otomotiv Teknolojileri Kongresi*ed. E. Solmaz, N. Kaya, F. Öztürk, Bursa, Turkey, May 26–27, 2014, Uludag University, Bursa, 2014.

12. D.K. Matlock and J.G. Speer, Processing opportunities for new advanced high-strength sheet steels, *Materials and Manufacturing Processes*, 25(1), 7–13, 2010.
13. D.K. Matlock, J.G. Speer, E.D. Moor, and P.J. Gibbs. Recent developments in advanced high strength sheet steels for automotive applications: An overview, *Journal of Engineering Science & Technology*, 15(1), 1–12, 2012.
14. S. Maggi and M. Murgia, Introduction to the metallurgic characteristics of advanced high strength steels for automobile applications, *Welding International*, 22, 610–618, 2008.
15. G. Weber, H. Thommes, H. Gaul, O. Hahn, and M. Rethmeier, Mechanical properties of weld bonded joints of advanced high strength steels, *Journal of Adhesion Science and Technology*, 25(18), 2369–2389, 2011.
16. O. Kwon, K. Lee, G. Kim, and K.G. Chin, New trends in advanced high strength steel developments for automotive applications, *Materials Science Forum*, 638–642, 136–141, 2010.
17. Q. Meng, J. Li, J. Wang, Z. Zhang, L. Zhang, Effect of water quenching process on microstructure and tensile properties of alloy cold rolled dual-phase steel, *Materials and Design*, 30, 2379–2385, 2009.
18. X. Cornet, and J. C. Herman, Method for making a multiphase hot-rolled steel strip, *U.S. Patent 0041933 A1*, 2003.
19. M. Dziedzic and S. Turczyn, Experimental and numerical investigation of strip rolling from dual phase steel, *Archives of Civil and Mechanical Engineering*, 21–30, 2010.
20. J. Adamczyk, A. Grajcar, Effect of heat treatment conditions on the structure and mechanical properties of DP-type steel, *Journal of Achievements in Materials and Manufacturing Engineering*, 305–308, 2006.
21. M. Calcagnotto, D. Ponge, D. Rabbe, Effect of grain refinement to 1 μm on strength and toughness of dual-phase steels, *Materials Science and Engineering A*, 527, 7832–7840, 2010.
22. X. Zuoa, Y. Chenb, M. Wangb, Study on Microstructures and Work Hardening Behaviour of Ferrite-Martensite Dual-Phase Steels with High-Content Martensite, *Materials Research*, 15(6), 915–921, 2012.
23. O.P. Ciuca, M. Ota, S. Deng, K. Ameyama, Harmonic Structure Design of a SUS329J1 Two Phase Stainless Steel and its Mechanical Properties, *Materials Transactions*, 54(9), 1629–1633, 2013.
24. Q. Meng, J. Li, H. Zheng, High-efficiency fast-heating annealing of a cold-rolled dual-phase steel, *Materials and Design*, 58, 194–197, 2014.

25. N. Saeidia, M. Karimib, M.R. Toroghinejada, Development of a new dual phase steel with laminated microstructural morphology**,** *Materials Chemistry and Physics*, 192, 1–7, 2017
26. M. Ota, K. Sawai, M. Kawakubo, S.K. Vajpai, K. Ameyama, Harmonic structure formation and deformation behavior in a (α + γ) two phase stainless steel, *6th International Conference on Nanomaterials by Severe Plastic Deformation IOP Publishing IOP Conf. Series: Materials Science and Engineering*, DOI:10.1088/1757-899X/63/1/012027, 2014.
27. T.S. Wang, Z. Li, B. Zhang, X.J. Zhang, J.M. Deng, F.C. Zhang, High tensile ductility and high strength in ultrafine-grained low-carbon steel, *Materials Science and Engineering A*, 527 (2010) 2798–2801, 2010.
28. P.D. Sudersanan, N. Kori, S. Aprameyan, U.N. Kempaiah, The effect of carbon content in martensite on the strength of dual phase steel, *International Journal of Industrial Engineering and Management Science*, 2, 1–4, 2012.
29. Q. Han, A. Asgari, P. D. Hodgson, and N. Stanford, "Strain partitioning in dual-phase steels containing tempered martensite," *Materials Science and Engineering A*, 611, 90–99, 2014.
30. B.P. Kumar and S.J. Babu, "Microstructure based Finite Element Analysis for Deformation Behavior of Aluminium based Metal Matrix Composite,"*International Journal for Engineering Research &Technology*, 2221–2223, 2014.
31. Q. Lai, O. Bouaziz, M. Goune, L. Brassart, M. Verdier, G. Parry, A. Perlade, Y.Brechet, T. Pardoen, "Damage and fracture of dual-phase steels: Influence of martensite volume fraction," *Materials Science and Engineering A*, 646, 322–331, 2015.
32. M. Ohata, M. Suzuki, A. Ui, and F. Minami, "3D-Simulation of ductile failure in two-phase structural steel with heterogeneous microstructure," *Engineering Fracture Mechanics*, 77(2), 277–284, 2010.
33. M. Singh, A. Das,T. Venugopalan, K. Mukherjee, M. Walnuj, T. Nanda, B.R. Kumar "Impact of Martensite Spatial Distribution on Quasi-Static and Dynamic Deformation Behavior of Dual-Phase Steel," *Metallurgical and Materials Transaction A*, 49(2), 463–475, 2018.
34. B. Ravi Kumar, N. K. Patel, K. Mukherjee, M. Walunj, G. K. Mandal, and T. Venugopalan, "Ferrite channel effect on ductility and strain hardenability of ultra high strength dual phase steel," *Materials Science and Engineering A*, 685, 187–193, 2017.
35. K. Ameyama and H. Fujiwara, "Creation of Harmonic Structure Materials with Outstanding Mechanical Properties," *Materials Science Forum*, 706–709, 9–16, 2012.
36. D. Orlov, H. Fujiwara, and K. Ameyama, "Obtaining Copper with Harmonic Structure for the Optimal Balance of Structure-Performance Relationship," *Materials Transactions*,

54(9), 1549–1553, 2013.

37. C. Sawangrat, O. Yamaguchi, S. K. Vajpai, and K. Ameyama, “Application of Harmonic Structure Design to Biomedical Co–Cr–Mo Alloy for Improved Mechanical Properties,” *Materials Transactions.*, 55, 99–105, 2014.
38. N. Z. Khalil, S. K. Vajpai, M. Ota, and K. Ameyama, “Application of Al-Si Semi-Solid Reaction for Fabricating Harmonic Structured Al Based Alloy,” *Materials Transactions*, 57, 1433–1439, 2016.
39. H. Fujiwara, R. Akada, Y. Yoshita, and K. Ameyama, “Microstructure and Mechanical Property of Nano-Duplex Materials Produced by HRS Process,” *Materials Science Forum*, 503–504, 227–232, 2006.
40. S.K. Vajpai, K. Ameyama, M. Ota, T. Watanabe, R. Maeda, T. Sekiguchi, G. Dirras, D. Tingaud, “High performance Ti-6Al-4V alloy by creation of harmonic structure design,” *IOP Conf. Ser. Materials Science and Engineering*, 63, 2014.
41. Z.H. Jiang, Z.Z. Guan, and J.S. Lian, “Effects of Microstructural Variables on the Deformation-Behavior of Dual-Phase Steel,” *Materials Science and Engineering*, 190, 1–2, 55–64, 1995.
42. A. Bag, K.K. Ray, and E.S. Dwarakadasa, “Influence of martensite content and morphology on tensile and impact properties of high-martensite dual-phase steels,” *Metallurgical and Materals Transaction A*, 30(5), 1193–1202, 1999.
43. Y. Mazaheri, A. Kermanpur, and A. Najafizadeh, “A novel route for development of ultrahigh strength dual phase steels,” *Materials Science and Engineering A*, 619, 1–11, 2014.
44. J. Zhang, H. Di, Y. Deng, and R.D.K. Misra, “Effect of martensite morphology and volume fraction on strain hardening and fracture behavior of martensite-ferrite dual phase steel,” *Materials Science and Engineering A*, 627, 230–240, 2015.
45. C.C. Tasan, M. Diehl, D. Yan, M. Bechtold, F. roters, L. Schemmann, C. Zheng, N. Peranio, D. Ponge, M. Koyama, K. Tsuzaki, D. Rabbe, “An Overview of Dual-Phase Steels: Advances in Microstructure-Oriented Processing and Micromechanically Guided Design,” *Annual Review of Materials Research*, 45, 1, 391–431, 2015.
46. W.J. Dan, Z.Q. Lin, S.H. Li, and W.G. Zhang, “Study on the mixture strain hardening of multi-phase steels,” *Materials Science and Engineering A*, 552, 1–8, 2012.
47. A. Ramazani, K. Mukherjee, U. Prahl, and W. Bleck, “Transformation-induced, geometrically necessary, dislocation-based flow curve modeling of dual-phase steels: Effect of grain size,” *Metallurgical and Materals Transaction A*, 43(10), 3850–3869,

2012.

48. M. Calcagnotto, D. Ponge, E. Demir, and D. Raabe, “Orientation gradients and geometrically necessary dislocations in ultrafine grained dual-phase steels studied by 2D and 3D EBSD,” *Materials Science and Engineering A*, 527, 10–11, 2738–2746, 2010.
49. A. Chakraborty, M. Adhikary, T. Venugopalan, V. Singh, T. Nanda, and B.R. Kumar, “Effect of ferrite-martensite interface morphology on bake hardening response of DP590 steel,” *Materials Science and Engineering A*, 676, 463–473, 2016.